

Spectroscopic Study on the Beryllium Abundances of Red Giant Stars *

Yoichi TAKEDA¹ and Akito TAJITSU²

¹*National Astronomical Observatory, 2-21-1 Osawa, Mitaka, Tokyo 181-8588*

takeda.yoichi@nao.ac.jp

²*Subaru Telescope, 650 N. A'ohoku Place, Hilo, HI 96720, U.S.A.*

tajitsu@subaru.naoj.org

(Received 2014 March 27; accepted 2014 June 27)

Abstract

An extensive spectroscopic study was carried out for the beryllium abundances of 200 red giants (mostly of late G and early K type), which were determined from the near-UV Be II 3131.066 line based on high-dispersion spectra obtained by Subaru/HDS, with an aim of investigating the nature of surface Be contents in these evolved giants; e.g., dependence upon stellar parameters, degree of peculiarity along with its origin and build-up timing. We found that Be is considerably deficient (to widely different degree from star to star) in the photosphere of these evolved giants by $\sim 1\text{--}3$ dex (or more) compared to the initial abundance. While the resulting Be abundances ($A(\text{Be})$) appear to weakly depend upon T_{eff} , $\log g$, $[\text{Fe}/\text{H}]$, M , *age*, and $v_e \sin i$, this may be attributed to the metallicity dependence of $A(\text{Be})$ coupled with the mutual correlation between these stellar parameters, since such tendencies almost disappear in the metallicity-scaled Be abundance ($[\text{Be}/\text{Fe}]$). By comparing the Be abundances (as well as their correlations with Li and C) to the recent theoretical predictions based on sophisticated stellar evolution calculations, we concluded that such a considerable extent/diversity of Be deficit is difficult to explain only by the standard theory of first dredge-up in the envelope of red giants, and that some extra mixing process (such as rotational or thermohaline mixing) must be responsible, which presumably starts to operate already in the main-sequence phase. This view is supported by the fact that appreciable Be depletion is seen in less evolved intermediate-mass B–A type stars near to the main sequence.

Key words: stars: abundances — stars: atmospheres — stars: evolution — stars: late-type

* Based on data collected at Subaru Telescope, operated by the National Astronomical Observatory of Japan.

1. Introduction

Beryllium (Be) is an astrophysically important light element like lithium (Li), which can be used as a probe of envelope mixing or as a proxy of stellar parameters such as age or rotational velocity, since it is destroyed when conveyed into hot deep interior owing to its fragility to nuclear reaction (burned in comparatively low temperatures of $\gtrsim 3.5 \times 10^6$ K). While it is not easy to determine the abundance of this element, since the strong resonance Be II doublet at the UV region of ~ 3131 Å is essentially the only abundance indicator available, a number of spectroscopic studies have been accumulated over these several decades (see, e.g., the Proceedings papers collected in Charbonnel et al. 2010 and the references therein), thanks to the availability of large telescopes built on ideal sites of high atmospheric transparency.

Nevertheless, most Be abundance studies published so far have been directed to main-sequence (or turn-off/subgiant) stars of mostly FGK types, and little is known about evolved stars such as red giants despite that several trials have been reported. That is, earlier-time studies (e.g., Boesgaard et al. 1977 for Hyades giants; De Medeiros et al. 1997 for Li-rich giants; Castilho et al. 1999 for Li-rich giants) appear to be less reliable in the quantitative sense because of the insufficient line list (the blending effect on the Be II 3131.06 line does not seem to be properly taken into account) as well as due to comparatively lower data quality, though all of them suggested a tendency of Be depletion. Meanwhile, more recent analyses by Melo et al. (2005) (for Li-rich giants) and Smiljanic et al. (2010) (several G-type giants in the moderately-young open cluster IC 4651) are considered to be more credible in this respect. Unfortunately, they failed to determine $A(\text{Be})^1$ of these giants, for which only the upper limit values could be estimated, since the Be II 3030–3131 doublet lines were found to be very weak almost near or below the detection limit (i.e, being essentially overwhelmed by blending of neighboring lines). Their work suggests that determining Be abundances in red giants (which seem considerably depleted in the general sense) is a difficult and challenging task, to say the least.

Takeda, Sato, and Murata (2008; hereinafter referred to as Paper I) carried out an extensive spectroscopic study on 322 late G and early K giants (targets of Okayama Planet Search Program) with various luminosities corresponding to mass range of $\sim 1.5\text{--}5 M_{\odot}$, and determined the stellar parameters as well as the chemical abundances of 17 elements in a consistent manner. Given that the properties of these red giants are well established, they make a good sample for investigating the connection between the surface abundance change of fragile light elements and the evolution-induced mixing in the envelope.

Along with this line, Liu et al. (2014) very recently investigated the behavior of Li abundances for a large sample of 378 G/K giants (where all 322 targets in Paper I are included),

¹ We define $A(\text{E})$ as the logarithmic abundance for an element E in the usual definition; i.e., $A(\text{E}) \equiv \log[N(\text{E})/N(\text{H})] + 12$.

and found the following characteristics:

- Li is heavily depleted in the surface of these stars. Actually, Li line is invisible in $\sim 1/3$ of the sample stars, for which only the upper limits of $A(\text{Li})$ could be assigned (ranging from $\lesssim 0$ to $\lesssim 1$).
- Even for the detection cases, $A(\text{Li})$ ranges between ~ 0.5 and ~ 2 , which means by ~ 1.5 – 3 dex underabundant relative to the solar-system abundance of $A_{\text{s.s.}}(\text{Li}) = 3.31$ (Anders & Grevesse 1989).
- Li line is undetected in all 23 planet-host stars, which implies that Li depletion tends to be enhanced by the existence of planets.
- Since the extent of deficiency is too large to be explained by the conventional stellar evolution theory for the first dredge-up in the red-giant phase (by as much as ~ 1.5 dex), a considerable portion of Li depletion may have taken place already at the main-sequence phase.

Thus, it is interesting to examine for these red-giant stars whether a similar trend is observed for Be, from the viewpoint of similarity in the characteristics of these two elements (though Li is burned in somewhat lower temperature at $T \gtrsim 2.5 \times 10^6$ K).

Admittedly, as mentioned above, it is not easy to extract information on Be abundances from the very weak and blended Be II feature in considerably Be-depleted cases (expected for evolved giants), especially when theoretical and observed spectra are compared simply by eye-judgement. Conveniently, however, we have experiences of Be abundance determination for a large sample of solar analog stars (Takeda et al. 2011, hereinafter referred to as Paper II), where an automatic solution-search algorithm to accomplish the best spectrum fitting in the neighborhood of the Be II 3131.066 line was applied to establish the Be abundance. Equipped with this technique, we decided to challenge studying the behaviors of Be abundances for a large number (200) of late G and early K-type giants, based on high-dispersion spectra obtained by observations with Subaru Telescope. The purpose of this paper is to report the results of this investigation.

The remainder of this article is organized as follows. After describing our observations and data reduction in section 2, we explain the procedures of our analysis (spectrum-fitting, equivalent-width derivation, and upper-limit estimation) in section 3. Section 4 is devoted to discussing the characteristics of the resulting Be abundances, especially in connection with stellar parameters and Li abundances, and the conclusion is summarized in section 5. Besides, we describe in appendix 1 additional numerical experiments, which were conducted on artificial spectra to study the nature of errors in our Be abundance determination. In appendix 2 are also presented the results of our supplementary Be II 3130–3131 doublet analysis for 5 late B through late A-type stars, which was carried out to get information on the surface Be abundances of intermediate-mass stars before reaching the red-giant phase.

2. Observational Data

All of the 200 targets in this investigation (see table 1) were selected from 322 late G or early K giants, which were already studied in detail in Paper I. The observations were carried out on 2013 July 17 and 19 (UT) with the High Dispersion Spectrograph (HDS; Noguchi et al. 2002) placed at the Nasmyth platform of the 8.2-m Subaru Telescope, by which high-dispersion spectra covering $\sim 3000\text{--}4600 \text{ \AA}$ could be obtained with two CCDs of $2\text{K}\times 4\text{K}$ pixels in the standard Ub setting with the blue cross disperser. We used the slit width of $0.''6$ ($300 \mu\text{m}$) and a binning of 2×2 pixels, which resulted in a spectrum resolving power of $R \simeq 60000$. The typical integrated exposure times was $\sim 5\text{--}10$ min for each star (typically $V \sim 5$).

The reduction of the spectra (bias subtraction, flat-fielding, scattered-light subtraction, spectrum extraction, wavelength calibration, co-adding of frames to improve S/N, continuum normalization) was performed by using the “echelle” package of the software IRAF² in a standard manner. Typical S/N ratios of $\sim 50\text{--}100$ (estimated from counts of photo-electrons; cf. table 1) were attained at the position of Be II 3130–3131 doublet lines in the finally resulting spectra.

3. Determination of Be Abundances

3.1. Spectrum Fitting Analysis

The strategy and the procedure of our Be abundance determination are almost the same as in Paper II, where we focus on the Be II 3131.066 line (weaker one of the doublet). Though this line is blended with Fe I 3131.043, it is still superior to the stronger Be II 3130.421 line which is severely contaminated by the strong V II+OH line feature at $\sim 3130.3 \text{ \AA}$. This situation is illustrated in figure 1, where observed spectra in the neighborhood of Be II doublet for two representative stars are simply compared with the theoretical spectra computed with various Be abundances.

Thus, our analysis is based on the synthetic spectrum fitting applied to the narrow region of 0.7 \AA width centered at 3131 \AA . Practically, we used the stellar spectrum analysis tool “MPFIT”, which was developed based on Kurucz’s (1993) ATLAS9/WIDTH9 program and has a function of establishing the spectrum-related parameters (elemental abundances, macrobroadening parameters, radial velocity, etc.) by automatically searching for the best-fit solutions without any necessity of precisely placing the continuum level in advance (Takeda 1995).³

² IRAF is distributed by the National Optical Astronomy Observatories, which is operated by the Association of Universities for Research in Astronomy, Inc. under cooperative agreement with the National Science Foundation.

³ In the present application to near-UV region heavily crowded with many spectral lines (and thus finding the line-free window is hopeless), it is essential to introduce not only the normalization constant (C) but also

We interpolated Kurucz’s (1993) grid of ATLAS9 model atmospheres in terms of T_{eff} , $\log g$, and $[\text{Fe}/\text{H}]$ (which were taken from Paper I) to generate the atmospheric model for each star. Then, given the photospheric model along with the microturbulence (v_t , also taken from Paper I), we determined for each star the abundances of three elements [$A(\text{Be})$, $A(\text{Ti})$, and $A(\text{Fe})$],⁴ along with the macrobroadening parameter (v_M ; e -folding half-width of the Gaussian macrobroadening function, $f_M(v) \propto \exp[(-v/v_M)^2]$) and the radial velocity shift, by applying the MPFIT program to the observed spectrum in the 3130.65–3131.35 Å region with the same line data as given in table 1 of Paper II. As in Paper II, we assumed LTE (local thermodynamical equilibrium) throughout this study.⁵

The solution of $A(\text{Be})$ (along with those of other parameters) turned out to converge for 130 stars (out of 200 targets in total). When $A(\text{Be})$ could not be determined (i.e., the solution did not converge because the Be II line is too weak), we neglected its contribution by assuming $A(\text{Be}) = -9.99$ and repeated the iteration to accomplish the fit. For these undetermined cases (70 stars), we estimated the upper limit values of $A(\text{Be})$ as described in the next subsection. The theoretical spectrum corresponding to the finally established parameter solutions is compared with the observed spectrum for each star in figure 2, where we can see that the agreement is mostly satisfactory.

It should be remarked that this is actually a very difficult analysis, since the contribution of the Be II line is not apparent but barely detectable only as a subtle second-order effect (even for the cases of well-established solutions). This situation is demonstrated in figure 3, where the observed spectra in the relevant region for stars with similar parameters but with appreciably different $A(\text{Be})$ solutions are compared with each other. As seen from this figure, the extent of Be abundance reflects on (i) the slight wavelength shift (toward redder for higher $A(\text{Be})$) of the Fe I 3131.043 + Be II 3131.066 line feature and (ii) the strength ratio of this Fe I+ Be II feature

the tilt-adjustment parameter (α) in comparing the observed flux (f_λ) with the theoretical flux (F_λ) in order to accomplish a satisfactory fit. That is, the right-hand side of equation (1) in Takeda (1995) is redefined as $\sum\{\log f_\lambda - \log F_\lambda - C - \alpha(\lambda - \lambda_{\text{min}})/(\lambda_{\text{max}} - \lambda_{\text{min}})\}/N$, and the best values of C and α are iteratively established, where λ_{max} and λ_{min} are the maximum and minimum wavelength of the relevant region.

⁴ The contributions of the lines of other elements (E) than these three were formally included by assuming the solar abundances scaled with the metallicity; i.e., $A(\text{E}) = A_\odot(\text{E}) + [\text{Fe}/\text{H}]$. Note also that we did not vary $A(\text{Nb})$ which was fixed (unlike the case in Paper II), since the Ti II 3130.810 line is much stronger than the Nb II 3130.780 line (the former dominating the Ti+Nb feature) in the spectra of red giants.

⁵ As done in Paper II (cf. the Appendix therein), we examined how the non-LTE effect is important on Be abundance determination for models with different T_{eff} (4500, 5000, 5500 K) and $\log g$ (1.5 and 3.0). We then found that the non-LTE correction ($\Delta \equiv A_{\text{NLTE}} - A_{\text{LTE}}$) is always positive (i.e., the non-LTE effect acts as a line-weakening) and quite sensitive to $\log g$ (but not to T_{eff}); i.e., $\Delta \lesssim 0.1\text{--}0.2$ dex ($\log g = 1.5$) and $\Delta \lesssim 0.05$ ($\log g = 3.0$). Accordingly, the extent of the non-LTE effect is somewhat larger for the present case of low-gravity red giants, as compared to the case of solar analogs in Paper II. Nevertheless, since corrections of such amount (on the order of ~ 0.1 dex at most) are not significant compared to the large diversity of $A(\text{Be})$ ($\gtrsim 2$ dex), we may neglect them without any serious problem.

to the neighboring Fe I 3131.25 line (larger for higher $A(\text{Be})$). However, the differences are too small to be confidently discernible by human eyes, though they can be discriminated by such a computer-based numerical judgement as adopted by us. Accordingly, the resulting solutions are generally very delicate and vulnerable to slight spectrum defect/noise, which means that they tend to suffer rather large uncertainties (especially near to the detection limit) though such ambiguities are difficult to quantify.

3.2. Equivalent Width and Upper Limit

As in Paper II, we prefer using equivalent widths (rather than the resulting abundance solutions themselves) which are easy to handle and useful in many respects.

We evaluated the (imaginary) equivalent width of the Be II 3131.066 line corresponding to the detection limit as $ew_{\text{BeII } 3131}^{\text{DL}} \simeq k \times \text{FWHM}/(\text{S/N})$, where k is a factor we assumed to be 2 according to our experience, S/N is the signal-to-noise ratio of the relevant spectrum (~ 50 –100), and FWHM was estimated from v_{M} as $\text{FWHM} \simeq 2\sqrt{\ln 2} (\lambda v_{\text{M}}/c)$ (c : velocity of light). Typical values of $ew_{\text{BeII } 3131}^{\text{DL}}$ are ~ 2 –5 mÅ (cf. table 1). Regarding 70 stars for which $A(\text{Be})$ could not be determined, we estimated its upper limit from $ew_{\text{BeII } 3131}^{\text{DL}}$.

Besides, we computed also for the $A(\text{Be})$ -established cases (130 stars) $EW_{\text{BeII } 3131}$ and $EW_{\text{FeI } 3131}$ “inversely” from the solutions of $A(\text{Be})$ and $A(\text{Fe})$ (resulting from the spectrum synthesis analysis) along with the adopted atmospheric model/parameters (cf. subsection 3.3 in Paper II). Then, considering that the reliability of $A(\text{Be})$ may be assessed by the relative comparison between $EW_{\text{BeII } 3131}$ and $ew_{\text{BeII } 3131}^{\text{DL}}$, we divided the results into four reliability classes (a, b, c, and x):

- class (a) \cdots reliable solution ($EW_{\text{BeII } 3131} > 3 \times ew_{\text{BeII } 3131}^{\text{DL}}$) [97 stars].
- class (b) \cdots less reliable solution ($3 \times ew_{\text{BeII } 3131}^{\text{DL}} > EW_{\text{BeII } 3131} > ew_{\text{BeII } 3131}^{\text{DL}}$) [28 stars].
- class (c) \cdots unreliable solution ($ew_{\text{BeII } 3131}^{\text{DL}} > EW_{\text{BeII } 3131}$) [5 stars].
- class (x) \cdots undetermined cases (only upper limit) [70 stars].

The final results of $EW_{\text{BeII } 3131}$ and $A(\text{Be})$ (or upper limits) along with the corresponding reliability classes are summarized in table 1. It is worth noting that class (a) results occupy the range of $A(\text{Be}) \gtrsim -1$ (see, e.g., figure 5), which is consistent with our numerical experiment (described in appendix 1), implying that Be abundance errors tend to become significant at $A(\text{Be}) \lesssim -1$.

Figure 4a shows a comparison between $A(\text{Fe})_{3131\text{fit}}$ (derived from this fitting) and $A(\text{Fe})_{EW}$ (already established in Paper I by using a number of Fe lines), which reveals that both correlate reasonably with each other, though considerable discrepancies are seen for several cases. The trend that $A(\text{Fe})_{3131\text{fit}}$ tends to be somewhat larger than $A(\text{Fe})_{EW}$ toward the metal-rich regime (where the Fe I 3131.043 line becomes stronger and more saturated) might be due to the depth-dependent microturbulence increasing with height in the low-density atmosphere of red giants (e.g., Takeda 1992), since we used v_t determined from lines of yellow region

(Paper I) while the forming depth of near-UV lines is comparatively higher.

According to figure 4b, where the strengths of Be II and Fe I lines at $\sim 3131 \text{ \AA}$ ($EW_{\text{BeII } 3131}$ and $EW_{\text{FeI } 3131}$) are compared with each other, we can recognize that $EW_{\text{BeII } 3131}$ widely vary from ~ 0 to $\sim 60 \text{ m\AA}$ while the Fe I line strength typically distributes around $EW_{\text{FeI } 3131} \sim 60\text{--}70 \text{ m\AA}$. As a result, the inequality relation $EW_{\text{BeII } 3131} \lesssim EW_{\text{FeI } 3131}$ mostly holds and the Fe I line tends to be predominant over the Be II line in the Fe I + Be II feature.

We also examined by using $EW_{\text{BeII } 3131}$ how the $A(\text{Be})$ results are sensitive to ambiguities in the adopted atmospheric parameters (T_{eff} , $\log g$, and v_t). Assuming $\pm 100 \text{ K}$, $\pm 0.2 \text{ dex}$, and $\pm 0.2 \text{ km s}^{-1}$ as typical uncertainties in T_{eff} , $\log g$, and v_t (see subsection 3.1 in Paper I, especially the comparison with literature values shown in figures 5–7 therein), we found that these perturbations caused changes in $A(\text{Be})$ by $\sim \pm 0.04 \text{ dex}$, $\sim \mp 0.12 \text{ dex}$, and $\lesssim 0.01 \text{ dex}$ (i.e., negligible), respectively. While the $\log g$ -sensitivity is comparatively large (due to the characteristic behavior in the line-strength of ionized species), we may generally state that errors in the atmospheric parameters are practically insignificant for the results of Be abundances.⁶

4. Discussion

4.1. Trend of Be Abundances

The final results of $A(\text{Be})$ derived from our analysis for 200 red giants are plotted against T_{eff} , $\log g$, $v_e \sin i$, $[\text{Fe}/\text{H}]$, M , and *age* in figures 5a–5f. In addition, in order to examine the extent of abundance peculiarity (or depletion degree) while removing the metallicity dependence in the initial abundance, similar plots with respect to $[\text{Be}/\text{Fe}]$ are also shown in figures 6a–6f, where $[\text{Be}/\text{Fe}]$ is the logarithmic Be abundance relative to the solar system (meteoritic) value of $A_{\text{s.s.}}(\text{Be}) = 1.42$ (Anders & Grevesse 1989) scaled with Fe ($[\text{Be}/\text{Fe}] \equiv A(\text{Be}) - 1.42 - [\text{Fe}/\text{H}]$).⁷ A close inspection of figure 5 suggests some rough trends regarding the dependence on stellar

⁶ For example, while our $\log g$ values tend to be systematically lower by $\sim 0.2\text{--}0.3 \text{ dex}$ in comparison with those published by other investigators (cf. Fig. 5–8 in Paper I), this influences $A(\text{Be})$ only by $\lesssim 0.2 \text{ dex}$, which is not important as compared with the observed large scatter.

⁷ It may be worth noting that the initial Be abundance of these intermediate-mass stars of population I ($-0.7 \lesssim [\text{Fe}/\text{H}] \lesssim +0.3$) may not have been simply proportional to the metallicity. That is, while the scaling relation between $A(\text{Be})$ and $[\text{Fe}/\text{H}]$ (as a result of Galactic chemical evolution) roughly holds over a wide metallicity range down to very metal-poor regime, the slope of $\delta A(\text{Be})/\delta [\text{Fe}/\text{H}]$ appears to be smaller than unity (i.e., ~ 0.5) as far as the metallicity range of disk stars ($-1 \lesssim [\text{Fe}/\text{H}]$) is concerned, as discussed in subsection 4.1 of Paper II. Nevertheless, $[\text{Be}/\text{Fe}]$ in the present definition is practically sufficient for the present purpose, since the metallicity span of our program stars is not large (i.e., only $\lesssim 1 \text{ dex}$). It is reasonable to regard the meteoritic result of $A_{\text{s.s.}}(\text{Be}) = 1.42$ as the initial Be abundance of a solar-metallicity star, since figure 8b of Paper II suggests $A(\text{Be}) \sim 1.5$ for this value. For reference, the solar photospheric Be abundance was estimated to be $A_{\odot}(\text{Be}) = 1.22$ in Paper II, where they concluded that a moderate decrease of $A(\text{Be})$ by $\sim 0.2\text{--}0.3 \text{ dex}$ has actually undergone in the solar envelope, ruling out the possibility of erroneous underestimation due to (controversial) UV missing opacity.

parameters: $A(\text{Be})$ tends to slightly increase with T_{eff} (figure 5a), $\log g$ (figure 5b), $v_e \sin i$ (figure 5c), $[\text{Fe}/\text{H}]$ (figure 5d), and M (figure 5e), while it shows a decreasing tendency with age (figure 5f).

We must recall here, however, that these parameters are not independent but correlated with each other. According to figure 3 of Paper I, lower mass (M) giants tend to be of lower luminosity, lower T_{eff} , older age , and lower $[\text{Fe}/\text{H}]$, while the M -dependence of $\log g$ is somewhat complicated (positive correlation in the global sense, but anti-correlation for $\sim 2\text{--}3 M_{\odot}$ stars belonging to the majority; cf. figure 3e therein). Besides, since the rotational velocity markedly slows down with a decrease in T_{eff} , $v_e \sin i$ systematically decreases with a decrease in M (cf. figures 10e and 10f in Paper I). This means that a dependence on one specific parameter may produce a spurious dependence on other parameters when they are correlated. In the present case, we consider that these apparent trends are essentially attributed to the metallicity dependence of $A(\text{Be})$ (figure 5d), since these tendencies almost disappear when we use $[\text{Be}/\text{Fe}]$ instead of $A(\text{Be})$, as we can recognize in figure 6.

4.2. Extent of Be Depletion and Its Implication

We can see from figure 5 and figure 6 that $A(\text{Be})$ shows a considerably large dispersion amounting to $\gtrsim 2$ dex, and that Be have suffered significant depletion (by $\sim 1\text{--}3$ dex with widely different degrees from star to star) in comparison to the initial Be abundance at the time of star formation. It would be interesting to compare this observed trend with theoretical predictions. In figure 6 are also shown the runs of $\log[X(^9\text{Be})/X_0(^9\text{Be})]$ (logarithmic depletion factor of surface ^9Be atoms relative to the initial composition) for 1.5, 2.5, and 4.0 M_{\odot} solar-metallicity ($Z = 0.014$) stars in the red-giant phase⁸ simulated by Lagarde et al. (2012) based on two different treatments of envelope mixing; i.e., standard treatment and treatment including rotational and thermohaline mixing. By comparing the observed $[\text{Be}/\text{Fe}]$ with such computed $\log[X(^9\text{Be})/X_0(^9\text{Be})]$ in figure 6, we can read the following characteristics and implications concerning the envelope-mixing process producing surface Be depletion:

— The extent of Be underabundance predicted by the conventional theory is only $\lesssim 1.5$ dex and thus quantitatively insufficient to account for the observed amount of depletion ($\sim 1\text{--}3$ dex), while the inclusion of rotational and thermohaline mixing produces more enhanced depletion (typically $\sim 2\text{--}2.5$ dex) which is closer to the observed tendency and thus comparatively preferable.

— Accordingly, we may state that only the canonical theory of first dredge-up is not sufficient, and extra mixing processes have to be additionally taken into consideration to explain the sur-

⁸ In order to avoid complexity caused by inclusion of near-main-sequence data, we restricted the theoretical plots (lines) only to those of the well-evolved red-giant stage satisfying the conditions of $T_{\text{eff}} < 5700$ K and $age > 10^{7.5}$ yr in figure 6 and figure 8. See figure 7 for the expected runs of $\log[X(^9\text{Be})/X_0(^9\text{Be})]$ during the whole evolutionary history. We also checked the results of calculations for a somewhat lower metallicity ($Z = 0.004$), but the differences were found to be insignificant.

face Be abundance trends of red giants.

— Since such a special mechanism (specifically, rotational mixing matters in this case, since thermohaline mixing is restricted to evolved red giants) begins to operate already at the main-sequence phase according to Lagarde et al.’s (2012) simulation (cf. figure 7), this means that Be anomaly (depletion) must have built up in the early-time of stellar evolution before reaching the red-giant phase.

— This consequence is ensured by another related observational fact. According to our supplementary analysis for five early-type stars of late B though late A-type stars (cf. appendix 2), which are progenitors of late G and early K giants having masses of $\sim 2.5\text{--}5 M_{\odot}$, most of them (4 out of 5) indicate significant Be deficiencies by $\gtrsim 0.5\text{--}1$ dex (cf. table 2). This evidence may lend support for the scenario that depletion of surface Be begins already in the main-sequence phase.

4.3. Comparison with Li and C

Finally, it is worthwhile to compare the Be abundances resulting from this study with those of Li (Liu et al. 2014) and C (Paper I) and to check the consistency with theoretical predictions, since both also suffer abundance changes by mixing of nuclear-processed products.

Regarding lithium, we can confirm that Li and Be share similar characteristics in several respects, which indicate that these two elements may have experienced similar depletion history in the envelope of red giants:

— The abundances of Be (derived in this study; based only on class-a results) and Li (from Liu et al. 2014; only “reliably determined” results were used) tend to show a reasonable correlation with each other, as shown in figure 8a ($A(\text{Be})$ vs. $A(\text{Li})$) and figure 8a’ ($[\text{Be}/\text{Fe}]$ vs. $[\text{Li}/\text{Fe}]$ ⁹). Actually, according to our linear-regression analysis applied to these data (filled circles in figure 8a and figure 8a’, excluding two outliers of HD 160781 and HD 212430), we found $A(\text{Be}) = 0.81(\pm 0.16) A(\text{Li}) - 1.00(\pm 0.17)$ with a correlation coefficient of $r = 0.66$, and $[\text{Be}/\text{Fe}] = 0.56(\pm 0.15) [\text{Li}/\text{Fe}] - 0.28(\pm 0.32)$ with a correlation coefficient of $r = 0.54$. Such a relation between the surface abundances of these two elements is also expected from Lagarde et al.’s (2012) theoretical simulation as shown in figure 8a’.

— The fact that Li line was not detected and only upper limit of $A(\text{Li})$ could be estimated for all the planet-host stars included in Liu et al.’s (2014) sample, is similarly seen for the present case of Be. That is, $A(\text{Be})$ could not be determined for 13 out of 15 planet-harboring stars in

⁹ We define $[\text{Li}/\text{Fe}] \equiv A(\text{Li}) - 3.31 - [\text{Fe}/\text{H}]$, where $A_{\text{s.s.}}(\text{Li}) = 3.31$ is the solar-system meteoritic abundance of Li (Anders & Grevesse 1989). Note that a remark similar to the case of Be (cf. footnote 7) should apply also to this case regarding this normalization in terms of the metallicity: i.e., it is not clear whether initial $A(\text{Li})$ scales with $[\text{Fe}/\text{H}]$. Nevertheless, it is reasonable to assume such a metallicity dependence (at $-1 \lesssim [\text{Fe}/\text{H}]$) according to chemical evolution calculations (see, e.g., figure 9 in Takeda & Kawonomoto 2005), though its observational confirmation is difficult because this element tends to be depleted with different degrees from star to star already in the main-sequence phase.

our sample (cf. table 1), which means that the non-detection probability is markedly higher than the case of non-planet-host stars.

— Given the existence of such Li–Be correlation, it is understandable that Liu et al. (2014) derived essentially the same consequence for Li (as we did for Be) regarding the build-up timing of abundance anomaly (beginning already at the main-sequence phase).

As to carbon, although a correlation between $A(\text{Be})$ and $A(\text{C})$ might be intuitively expected since mixing-induced deficit of Be should be accompanied by a decrease of C (due to mixing of CN-cycled products), this would not be easy to detect according to Lagarde et al.’s (2012) calculation, since $[\text{C}/\text{Fe}]$ does not monotonically correlate with $[\text{Be}/\text{Fe}]$ (i.e., changing in a somewhat complex manner) and the variation range of the former is appreciably smaller than the latter as illustrated in figure 8b’. Thus, it is no wonder that any meaningful correlation is not observed between Be and C in figure 8b and figure 8b’ (the correlation coefficient is $r \simeq 0.1$, based on the class-a results). Still, given that the extents of observed $[\text{Be}/\text{Fe}]$ and $[\text{C}/\text{Fe}]$ are favorably compared with the theoretical predictions (cf. figure 8b’), we may state that our results are well reasonable.

5. Conclusion

An extensive spectroscopic study was conducted for establishing the Be abundances of 200 red giants (mostly of late G and early K type) in order to investigate the behaviors of the surface abundances of this fragile element and their implications; e.g., whether they are normal or peculiar, how they depend on various stellar parameters, how they suffer the depletion process such as evolution-induced envelope mixing.

Based on high-dispersion spectra obtained with Subaru/HDS, we analyzed the narrow wavelength region in near UV comprising the Be II 3131.066 line (blended with the Fe I 3131.043 line) by using the spectrum-synthesis technique along with the automatic solution-search approach (already adopted in Paper II), where the stellar parameters of target stars were taken from Paper I.

It turned out that this Be II line is considerably weakened (due to the general tendency of Be depletion) and dominated by the neighboring Fe I line in most cases, which makes the analysis difficult. Actually, while we could somehow arrive at converged solution of $A(\text{Be})$ for 130 stars, its determination failed for the rest of 70 stars, for which only upper limits were estimated.

The resulting $A(\text{Be})$ was found to slightly depend upon stellar parameters, in the sense that it tends to decline (i.e., Be depletion being more enhanced) somewhat with increasing *age* as well as with a decrease in T_{eff} , $\log g$, $v_e \sin i$, $[\text{Fe}/\text{H}]$, and M . However, since these apparent trends almost disappear when use use $[\text{Be}/\text{Fe}]$ instead of $A(\text{Be})$, they are considered to be due to the metallicity dependence of $A(\text{Be})$ coupled with the mutual dependence of these stellar parameters.

We found that $A(\text{Be})$ as well as $[\text{Be}/\text{Fe}]$ show a considerably large dispersion amounting to $\gtrsim 2$ dex, and that Be has suffered significant depletion by $\sim 1\text{--}3$ dex (or even more for non-detection cases) compared to the expected initial abundance.

Consulting Lagarde et al.’s (2012) theoretical simulations, we found that the expected extent of Be underabundance based on the conventional theory (only by $\lesssim 1.5$ dex) is quantitatively insufficient, while the inclusion of rotational and thermohaline mixing predicts more enhanced depletion (typically by $\sim 2\text{--}2.5$ dex) being closer to the required amount. This implies that only the canonical theory of first dredge-up is not sufficient and extra mixing processes have to be additionally taken into consideration.

Since such special mixing mechanisms begin to operate already at the main-sequence phase, appreciable Be anomaly must have built up in the early-time of stellar evolution before reaching the red-giant phase. This view is also supported by our supplementary analysis for late B and A-type stars, for which we found significant Be deficiencies by $\gtrsim 0.5\text{--}1$ dex.

We confirmed a reasonable correlation between the abundances of Be and Li, which is consistent with the theoretical prediction. Besides, since $A(\text{Be})$ could not be determined for most (13 out of 15) planet-harboring stars, Be depletion appears to be enhanced by the existence of giant planets, which was also reported by Liu et al. (2014) for the case of Li. Accordingly, given that Li and Be share similar characteristics, they may have experienced similar depletion history.

As to carbon, although we could not detect any meaningful correlation between Be and C (contrary to our naive expectation), this is understandable because both correlate (not monotonically but) only in a somewhat complex manner with each other. At any event, the extents of observed $[\text{Be}/\text{Fe}]$ and $[\text{C}/\text{Fe}]$ are reasonably consistent with the theoretical predictions.

We express our heartfelt thanks to an anonymous referee for a number of valuable comments and suggestions, which were of great help in improving the contents of this paper.

Appendix 1. Accuracy-Check Experiment on Artificial Spectra

In order to understand the nature of errors involved in our Be abundance determination procedure using the synthetic spectrum-fitting technique, we carried out supplementary numerical experiments. Adopting $T_{\text{eff}} = 4900$ K, $\log g = 2.5$, $[\text{Fe}/\text{H}] = 0.0$, $v_t = 1.5$ km s $^{-1}$, and $v_M = 5$ km s $^{-1}$ as the representative set of parameters, we first computed theoretical spectra for six different beryllium abundances ($A(\text{Be}) = -1.5, -1.0, -0.5, 0.0, +0.5, \text{ and } +1.0$), for which the corresponding $EW_{\text{BeII } 3131}$ values are 2.4, 7.3, 20.1, 45.3, 76.1, and 104.1 mÅ, respectively (while $EW_{\text{FeI } 3131}$ is 66.2 mÅ in this case). Then, randomly-generated noises of normal distribution (corresponding to $S/N = 100, 50, \text{ and } 20$) were added to them, and this process was repeated 100 times for each of the 18 ($= 6 \times 3$) cases. In this way, 1800 artificial spectra with different combinations of ($A(\text{Be}), S/N$) were generated. Next, we tried Be abundance determination in

exactly the same manner as described in subsection 3.1 for each spectrum. From the resulting many $A(\text{Be})$ solutions for each ($A(\text{Be})$, S/N) combination, the average ($\langle A(\text{Be}) \rangle$) as well as the standard deviation (σ) were derived as presented in table 2, where the number of successfully determinations among 100 trials (N) is also given.

Inspecting this table 2, we can see several characteristic trends regarding abundance errors in terms of $A(\text{Be})$ and S/N.

— The abundance error (σ) progressively increases with a decrease in $A(\text{Be})$ as well as in S/N (though the averaged abundances are almost consistent with the given ones), which is naturally understandable.

— Especially, an appreciable error-enhancement is noticeable when $A(\text{Be})$ drops below ~ -1 .

— Even cases where Be abundance is undeterminable (i.e., the iterative solution never converged) gradually appear at $A(\text{Be}) \lesssim -1$.

Accordingly, we may roughly state that $A(\text{Be}) \sim -1$ is nearly the critical border with respect to the reliability of Be abundances we determined in section 3, in the sense that significant errors may be involved in the results of $A(\text{Be}) \lesssim -1$ while those of $A(\text{Be}) \gtrsim -1$ have comparatively higher reliability. This conclusion is reasonably consistent with the classification defined in subsection 3.2, because the lower envelope of class (a) is located around $A(\text{Be}) \sim -1$ where class (b) abundances also overlap (cf. figure 5).

Appendix 2. Beryllium in Early-Type Stars

In order to understand the nature of Be depletion observed in G–K giants of intermediate mass ($\sim 2\text{--}5 M_{\odot}$), it is important to get information on the surface Be abundances of unevolved late B–A stars near to the main sequence (corresponding to the relevant mass range). Although several observational studies on Be abundances of upper-main sequence stars were published in 1970–1980s, which were mainly motivated by interest on the chemical peculiarities in HgMn stars (where Be tends to be conspicuously overabundant in many cases), they were based on low-quality spectra of photographic plates or IUE satellite. Actually, Be II 3130–3131 doublet lines could not be detected for normal (i.e., non-HgMn) late B–A type stars, for which only upper limits were derived, in these pioneering investigations (see, e.g., Boesgaard et al. 1982).

Given this situation, we tried Be abundance determinations for five late B–A stars (see table 2 for the list) corresponding to $\sim 2\text{--}5 M_{\odot}$ (cf. their positions on the HR diagram shown in figure 9), since their high-quality Subaru/HDS spectra were available to us. Most of the observational data were obtained on 2013 July 19 (UT), except for Vega which was observed on 2010 May 25 (UT), with the same setting as adopted for our 200 main targets. Regarding the atmospheric parameters, T_{eff} and $\log g$ were determined from the colors of Strömberg’s *uvby β* photometric system with the help of the *uvbybetanew*¹⁰ program (Napiwotzki et al. 1993) as

¹⁰ <http://www.astro.le.ac.uk/~rn38/uvbybeta.html>.

done in Takeda et al. (2009), while we assumed reasonable values of v_t (1, 2, and 4 km s⁻¹) by consulting the empirical v_t vs. T_{eff} formula (cf. equation (1) in Takeda et al. 2009)

Our analysis was done in a similar manner as described in subsection 3.1, except that spectrum fitting was done in a wider wavelength range (3128–3132.5 Å) and OH molecular lines were neglected. We could somehow get the solution of $A(\text{Be})$ converged for all 5 stars as presented in table 2. However, except for 15 Vul exhibiting sufficiently strong Be II 3130/3131 doublet, detections of these lines are delicate and uncertain for other 4 stars, as shown in figure 10. As a matter of fact, $EW_{\text{BeII } 3131}$ (equivalent width of the Be II 3131.066 line; cf. subsection 3.2) corresponding to the solution of $A(\text{Be})$ was evaluated as 1.1, 3.2, 0.6, 76.8, and 4.3 mÅ for π Cet, α Lyr, o Peg, 15 Vul, and HD 186377, respectively. Since the detection limit ($ew_{\text{BeII } 3131}^{\text{DL}}$) is on the order of several to ~ 10 mÅ in this case, the $A(\text{Be})$ results for these 4 stars (π Cet, α Lyr, o Peg, and HD 186377) are subject to considerable uncertainties (class (c) according to the classification in subsection 3.2) and had better be regarded rather as upper limits.

Keeping this in mind, we conclude the following characteristics regarding the Be abundances of these stars.

— Given the results that $A(\text{Be}) \lesssim 0.8\text{--}0.9$ (π Cet and α Lyr) $A(\text{Be}) \lesssim 0$ (o Peg), and $A(\text{Be}) \lesssim -0.4$ (HD 186377), 4 (out of 5) stars of our sample show significant Be deficiencies by $\gtrsim 0.5\text{--}2$ dex to different degrees from star to star, as compared to the initial Be abundance of $A(\text{Be}) \sim 1.5$ (cf. subsection 4.1).

— Only one star (15 Vul), for which we obtained $A(\text{Be}) \simeq 1.5$, seems to retain the initial Be abundance without any anomaly, which is interesting. Yet, we had better bear in mind a possibility that this star might have been a HgMn star with overabundant Be when it was on the main sequence.

— To sum up, while the surface Be abundances of these late B–A stars are considerably diversified, we may generally state that Be tends to be significantly underabundant, which implies that some kind of depletion process takes place already in the main-sequence phase.

References

- Anders, E., & Grevesse, N. 1989, *Geochim. Cosmochim. Acta*, 53, 197
Arenou, F., Grenon, M., & Gómez, A. 1992, *A&A*, 258, 104
Boesgaard, A. M., Heacox, W. D., & Conti, P. S. 1977, *ApJ*, 214, 124
Boesgaard, A. M., Heacox, W. D., Wolff, S. C., Borsenberger, J., & Praderie, F. 1982, *ApJ*, 259, 723
Castilho, B. V., Spite, F., Barbuy, B., Spite, M., De Medeiros, J. R., & Gregorio-Hetem, J. 1999, *A&A*, 345, 249
Charbonnel, C., Tosi, M., Primas, F., & Chiappini, C. (eds.) 2010, *Light Elements in the Universe*, Proc. IAU Symp. 268 (Cambridge: Cambridge University Press)
De Medeiros, J. R., Lèbre, A., de Garcia Maia, M. R., & Monier, R. 1997, *A&A*, 321, L37
Flower, P. J. 1996, *ApJ*, 469, 355

- Kurucz, R. L. 1993, Kurucz CD-ROM, No. 13 (Harvard-Smithsonian Center for Astrophysics)
- Lagarde, N., Decressin, T., Charbonnel, C., Eggenberger, P., Ekström, S., & Palacios, A. 2012: A&A 543, A108
- Lejeune, T., & Schaerer, D. 2001, A&A, 366, 538
- Liu, Y. J., Tan, K. F., Wang, L., Zhao, G., Sato, B., Takeda, Y., & Li, H. N. 2014, ApJ, 785, 94
- Melo, C. H. F., de Laverny, P., Santos, N. C., Israelian, G., Randich, S., do Nascimento Jr, J. D., & De Medeiros, J. R. 2005, A&A, 439, 227
- Napiwotzki, R., Schönberner, D., & Wenske, V. 1993, A&A, 268, 653
- Noguchi, K., et al. 2002, PASJ, 54, 855
- Smiljanic, R., Pasquini, L., Charbonnel, C., & Lagarde, N. 2010, A&A, 510, A50
- Takeda, Y. 1992, A&A, 253, 487
- Takeda, Y. 1995, PASJ, 47, 287
- Takeda, Y., Kang, D.-I., Han, I., Lee, B.-C., & Kim, K.-M. 2009, PASJ, 61, 1165
- Takeda, Y., & Kawanomoto, S. 2005, PASJ, 57, 45
- Takeda, Y., Sato, B., Murata, D. 2008, PASJ, 60, 781 (Paper I)
- Takeda, Y., Tajitsu, A., Honda, S., Kawanomoto, S., Ando, H., & Sakurai, T. 2011, PASJ, 63, 697 (Paper II)
- van Leeuwen, F. 2007, Hipparcos, the New Reduction of the Raw Data (Berlin: Springer)

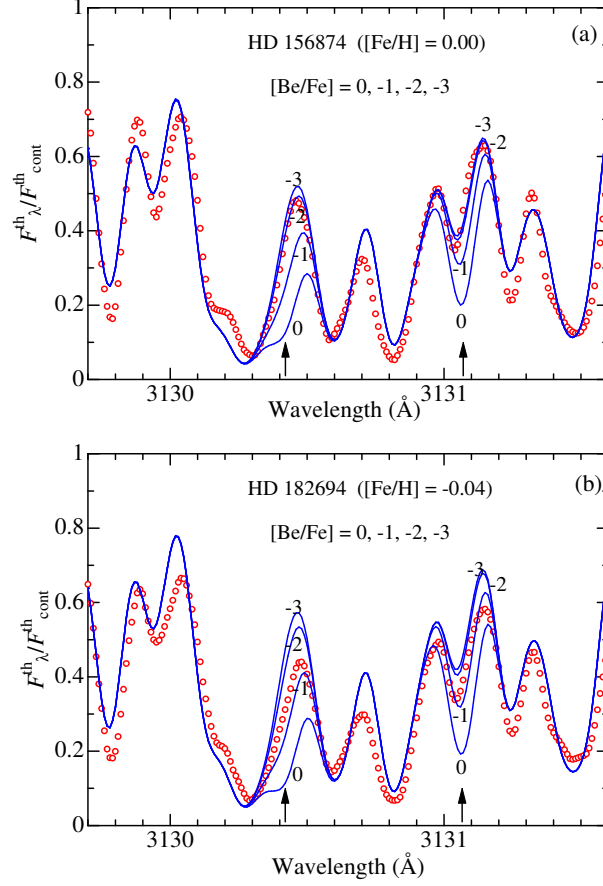


Fig. 1. Examples of comparison between the observed spectrum (red open circles; normalized by an appropriately assigned continuum level) and the theoretical simulation (blue solid lines; $F_{\lambda}^{\text{th}}/F_{\text{cont}}^{\text{th}}$) in the wavelength region comprising Be II 3130.421 and 3131.066 lines. The upper panel (a) shows the undetermined case (HD 156874; $A(\text{Be})$ did not converge) and the lower panel (b) corresponds to the determinable case (HD 182694; $A(\text{Be})$ converged). The theoretical spectrum is synthesized basically with the metallicity-scaled solar abundances ($[X/\text{Fe}] = 0$) and broadened with $v_{\text{M}} = 5 \text{ km s}^{-1}$, but four different $A(\text{Be})$ values ($[\text{Be}/\text{Fe}] = 0, -1, -2, -3$) are assigned to show its effect.

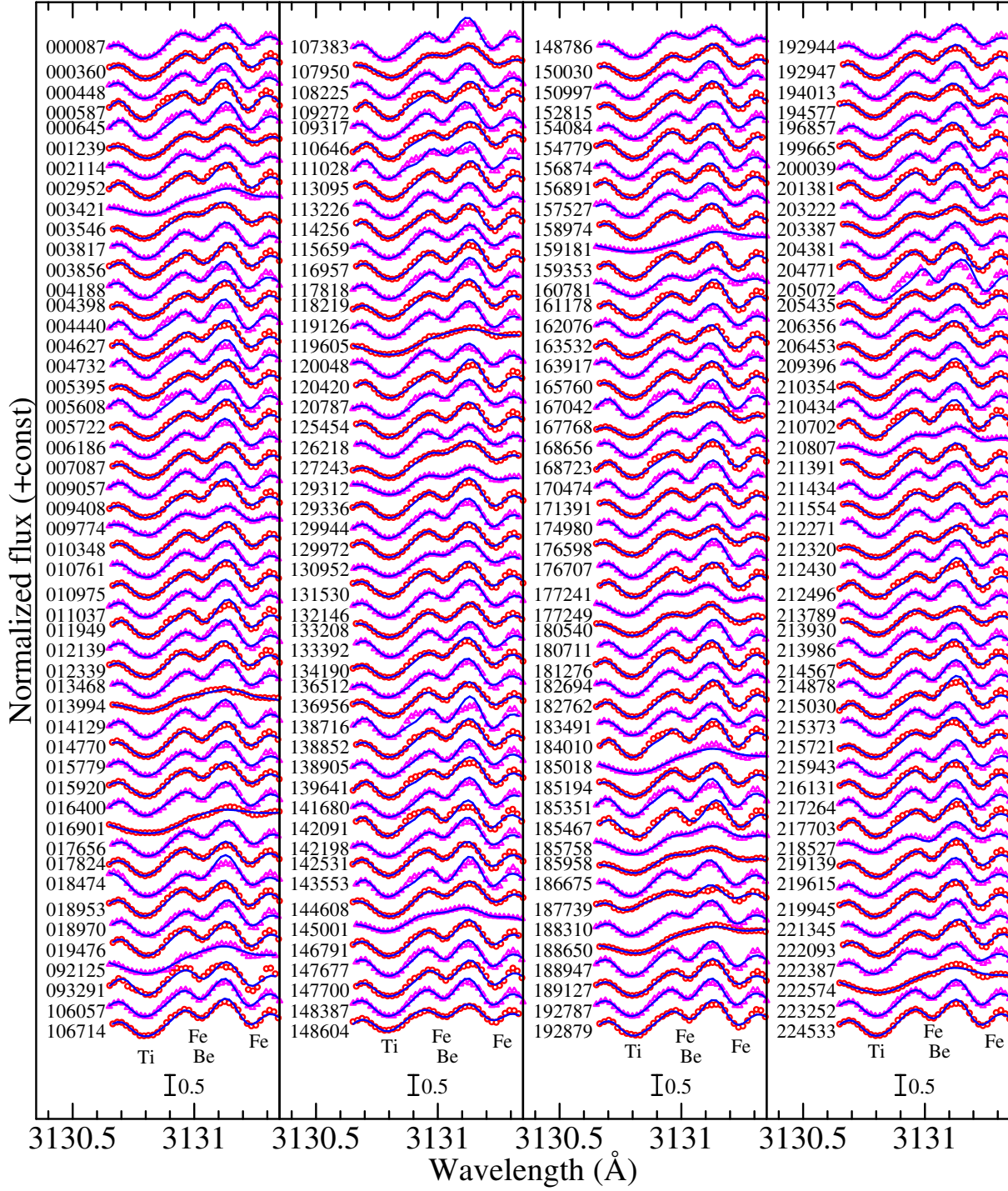


Fig. 2. Synthetic spectrum fitting in the 3130.65–3131.35 Å region for all of the 200 targets. The best-fit theoretical spectra are shown by solid lines, while the observed data are plotted by open circles. A vertical offset of 0.5 is applied to each relative to the adjacent ones. Each of the spectra are arranged in the increasing order of HD number (indicated on the left to each spectrum). The wavelength scale of each spectrum is adjusted to the laboratory system.

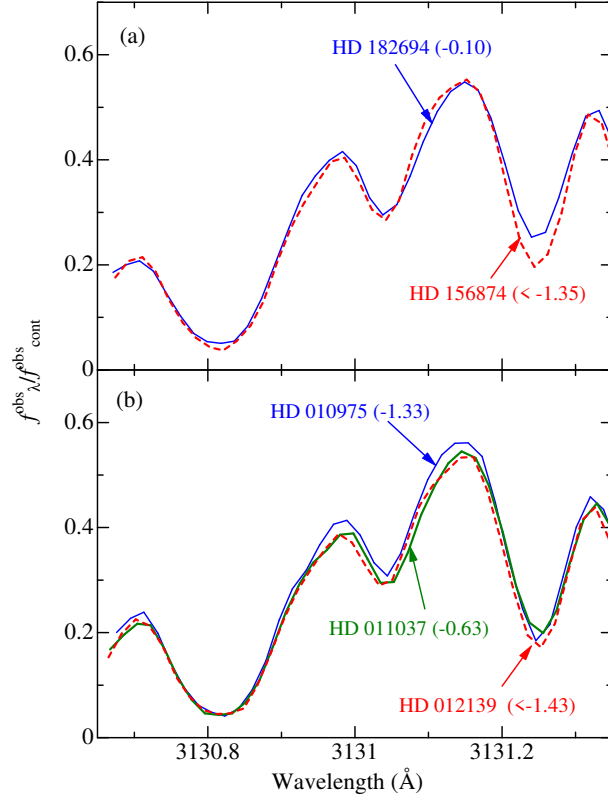


Fig. 3. Demonstration that only very subtle changes are recognizable in the observed spectra (in the Be II 3131.07 region) for stars with similar parameters but with appreciably different $A(\text{Be})$. (a) HD 182694 and HD 156874 (see also figure 1). (b) HD 10975, HD 11037, and HD 12139. The corresponding $A(\text{Be})$ values are also indicated after the star names. The continuum of the observed spectra ($f_{\text{cont}}^{\text{obs}}$) used here for the normalization was evaluated in reference to the theoretical continuum ($F_{\text{cont}}^{\text{th}}$), while using the solutions of C and α (cf. footnote 3) derived as by-products of spectrum fitting.

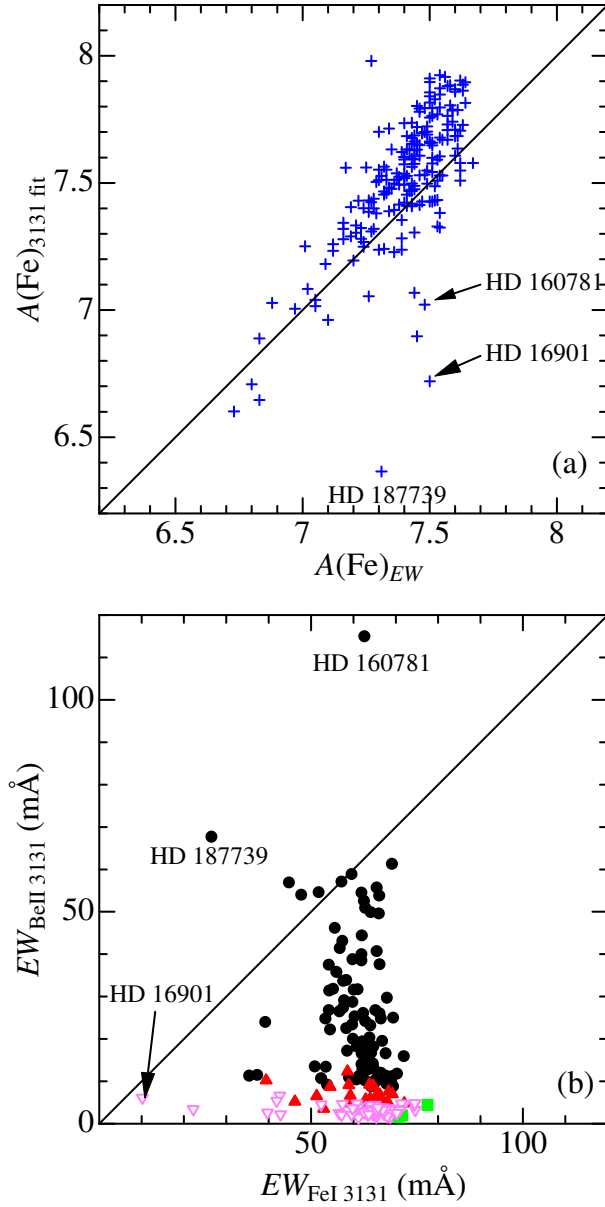


Fig. 4. (a) Correlation of the Fe abundance derived from the synthetic spectrum fitting analysis in the 3130.65–3131.35 Å region (this study) with that determined based on EW s of many Fe lines (cf. Paper I). (b) Comparison of $EW_{\text{FeI } 3131.043}$ and $EW_{\text{BeII } 3131.066}$ (equivalent widths inversely computed from fitting-based abundance solutions of Fe and Be). Symbols indicate the relevant reliability class for the $A(\text{Be})$ solution (cf. caption in figure 5). Note that upper-limit values of $EW_{\text{BeII } 3131}$ are plotted here for undetermined cases (class x; pink downward triangle)

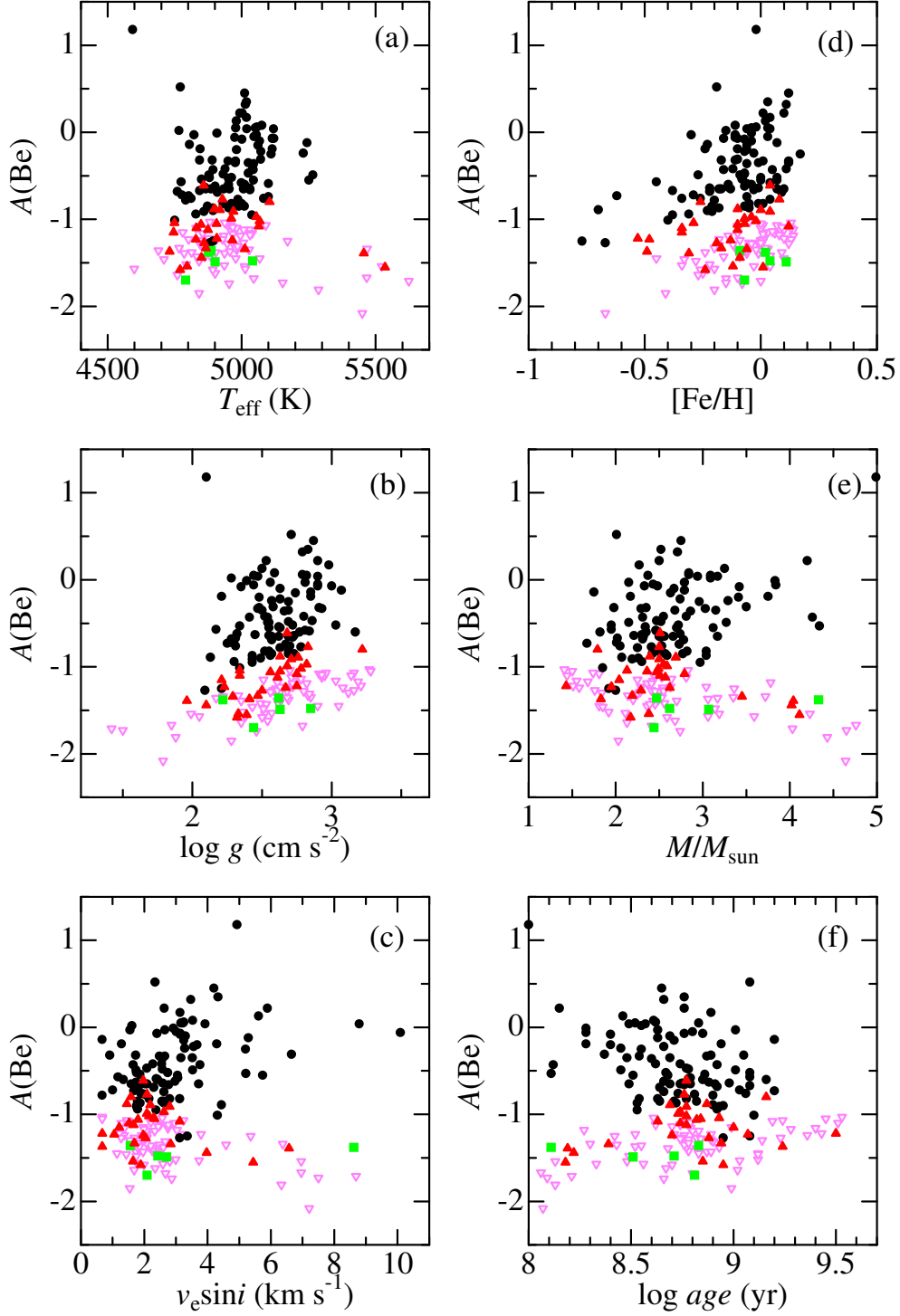


Fig. 5. Beryllium abundances of the program stars plotted against six stellar parameters presented in table 1: (a) T_{eff} , (b) $\log g$, (c) $v_e \sin i$, (d) $[\text{Fe}/\text{H}]$, (e) M , and (f) age . Black filled circles ... reliable abundances (class a); red filled triangles ... less reliable abundances (class b) green squares ... unreliable results near/below the detection limit (class c); pink downward triangles ... upper-limit values for the undetermined cases (class x). See subsection 3.2 for more details regarding this classification.

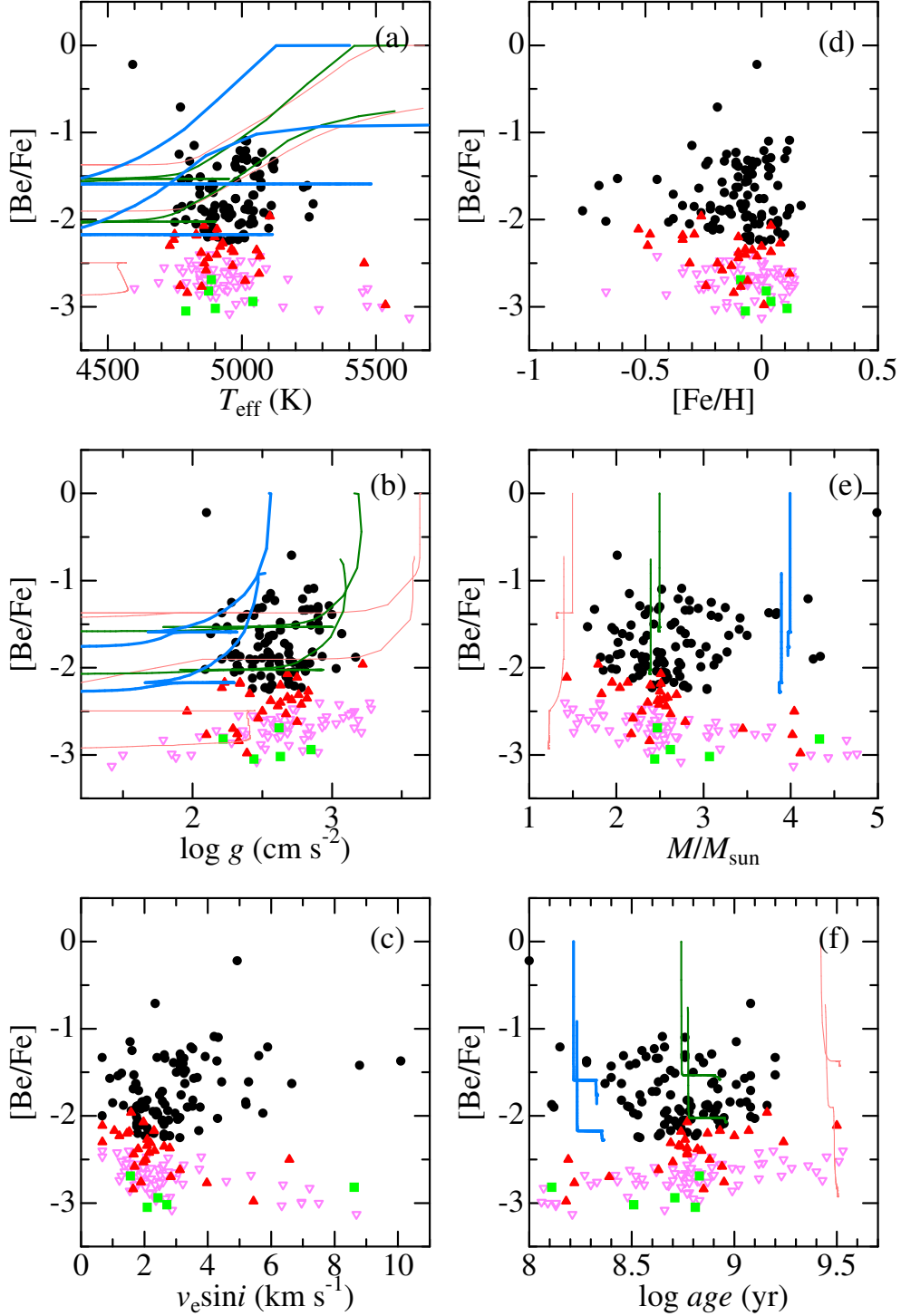


Fig. 6. $[\text{Be}/\text{Fe}]$ (metallicity-scaled logarithmic Be abundances relative to the solar-system composition) of the program stars plotted against six stellar parameters, arranged in the same manner as in figure 5. See the caption of figure 5 for the meanings of the symbols. In panels (a), (b), (e), and (f), Lagarde et al.’s (2012) theoretically simulated results of $\log[X(^9\text{Be})/X_0(^9\text{Be})]$ (logarithmic surface abundance of ^9Be relative to the initial composition), in the red-giant phase for the solar metallicity ($Z = 0.014$) are also depicted for comparison, where stellar masses are discriminated by line thickness (thin orange line, normal green line, and thick blue lines correspond to 1.5 , 2.5 , and $4.0 M_{\odot}$, respectively). Note that two kinds of curves are shown corresponding to different treatments of envelope mixing; i.e., standard treatment and treatment including rotational and thermohaline mixing. Although these two sets are drawn in the same line-type, they are discernible as the latter generally shows appreciably lower Be abundances by 0.5 – 1.0 dex as compared to the former. In panel (e), the curves of the latter set are slightly shifted by $-0.1 M_{\odot}$ in order to avoid degeneracy.

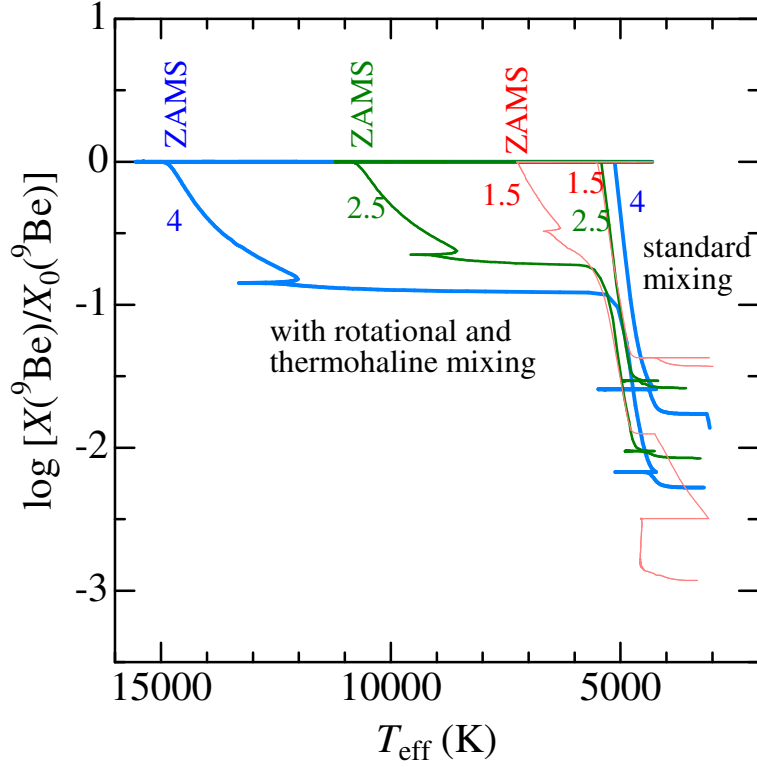


Fig. 7. Run of $\log[X(^9\text{Be})/X_0(^9\text{Be})]$ (logarithmic surface abundance of ^9Be relative to the initial composition), theoretically simulated along the whole evolutionary sequence (Lagarde et al. 2012), plotted against T_{eff} . As in figures 6 (and figure 8), shown here are the results corresponding to three stellar masses of 1.5, 2.5, and 4.0 M_{\odot} for two different treatments of envelope mixing: (i) standard treatment, (ii) treatment including rotational and thermohaline mixing. See the caption of figure 6 for the meaning of the line-type.

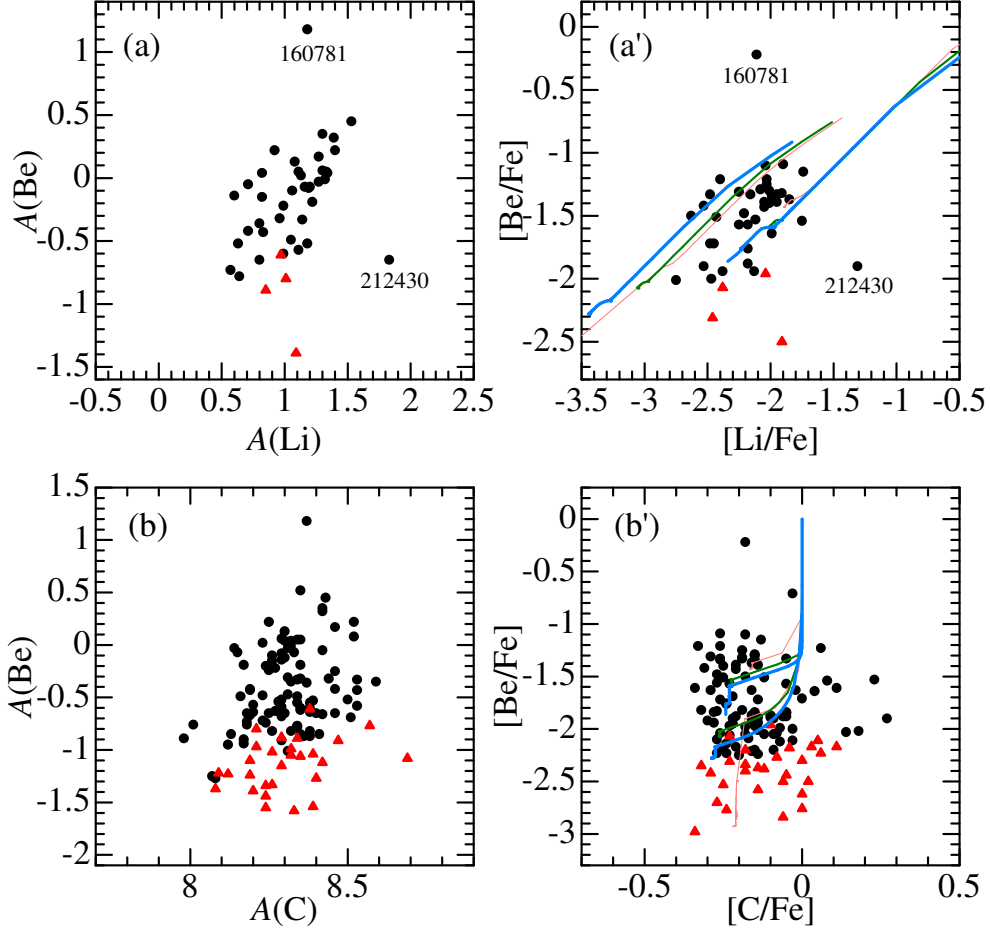


Fig. 8. Beryllium abundances plotted against the abundances of other two key elements; Li (upper panels) and C (lower panels). The left panels give the direct comparison of $A(X)$ (X is Li or Be or C), while the right panels show the mutual correlations of $[X/\text{Fe}]$ (metallicity-scaled logarithmic abundance relative to the solar composition [for C] or solar-system composition [for Li and Be]). The data of $A(\text{Li})$ are taken from Liu et al. (2014; only the results which they classified as “reliably determined” were used), while those of $A(\text{C})$ are from Paper I. Note that we show only the reliable (class a) as well as less reliable (class b) $A(\text{Be})$ values here (disregarding unreliable results as well as upper-limit cases). The meanings of the symbols are the same as in figure 5. In the right panels (a' and b'), the correlations of Lagarde et al.'s (2012) theoretically simulated results of $\log[X(^7\text{Li})/X_0(^7\text{Li})]$, $\log[X(^9\text{Be})/X_0(^9\text{Be})]$, and $\log[X(^{12}\text{C})/X_0(^{12}\text{C})]$ are also shown (see the caption in figure 6 for the meaning of the line-type).

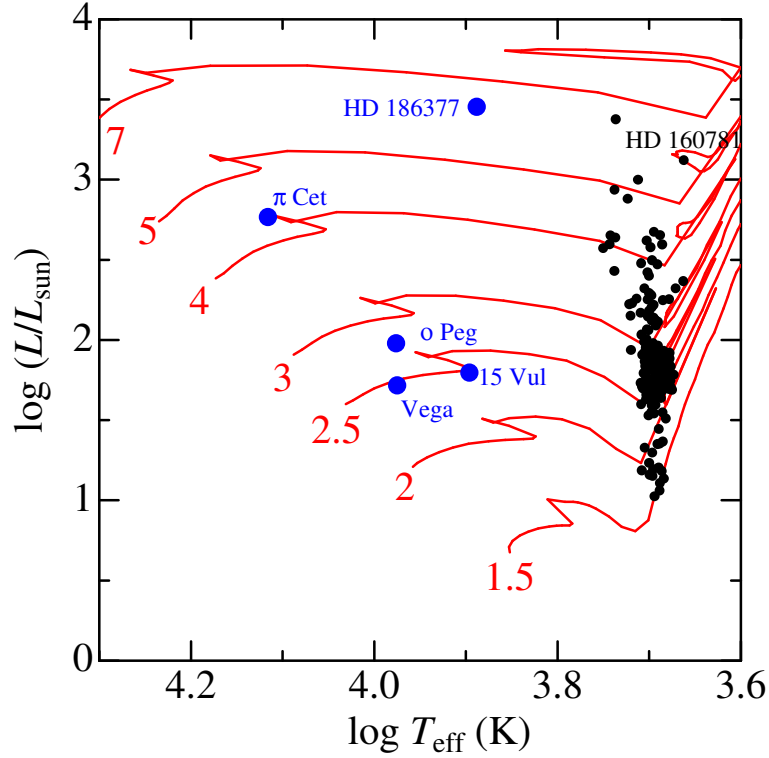


Fig. 9. Five late B–late A stars (the targets of our supplementary analysis) are plotted on the theoretical HR diagram ($\log(L/L_{\odot})$ vs. $\log T_{\text{eff}}$) by blue filled circles, where 200 program stars of red giants are also shown by black dots for comparison. The effective temperature (T_{eff}) was determined from $uvby\beta$ photometry as described in the text, and the bolometric luminosity (L) was evaluated from the apparent visual magnitude, Hipparcos parallax (van Leeuwen 2007), Arenou, Grenon, and Gómez’s (1992) interstellar extinction map, and Flower’s (1996) bolometric correction. Theoretical evolutionary tracks corresponding to the solar metallicity computed by Lejeune and Schaerer (2001) for seven different initial masses (1.5, 2, 2.5, 3, 4, 5, and 7 M_{\odot}) are also depicted by red lines. Along with the five targets, the position of HD 160781 (K giant with an exceptionally high Be abundance of $A = +1.18$) is also indicated.

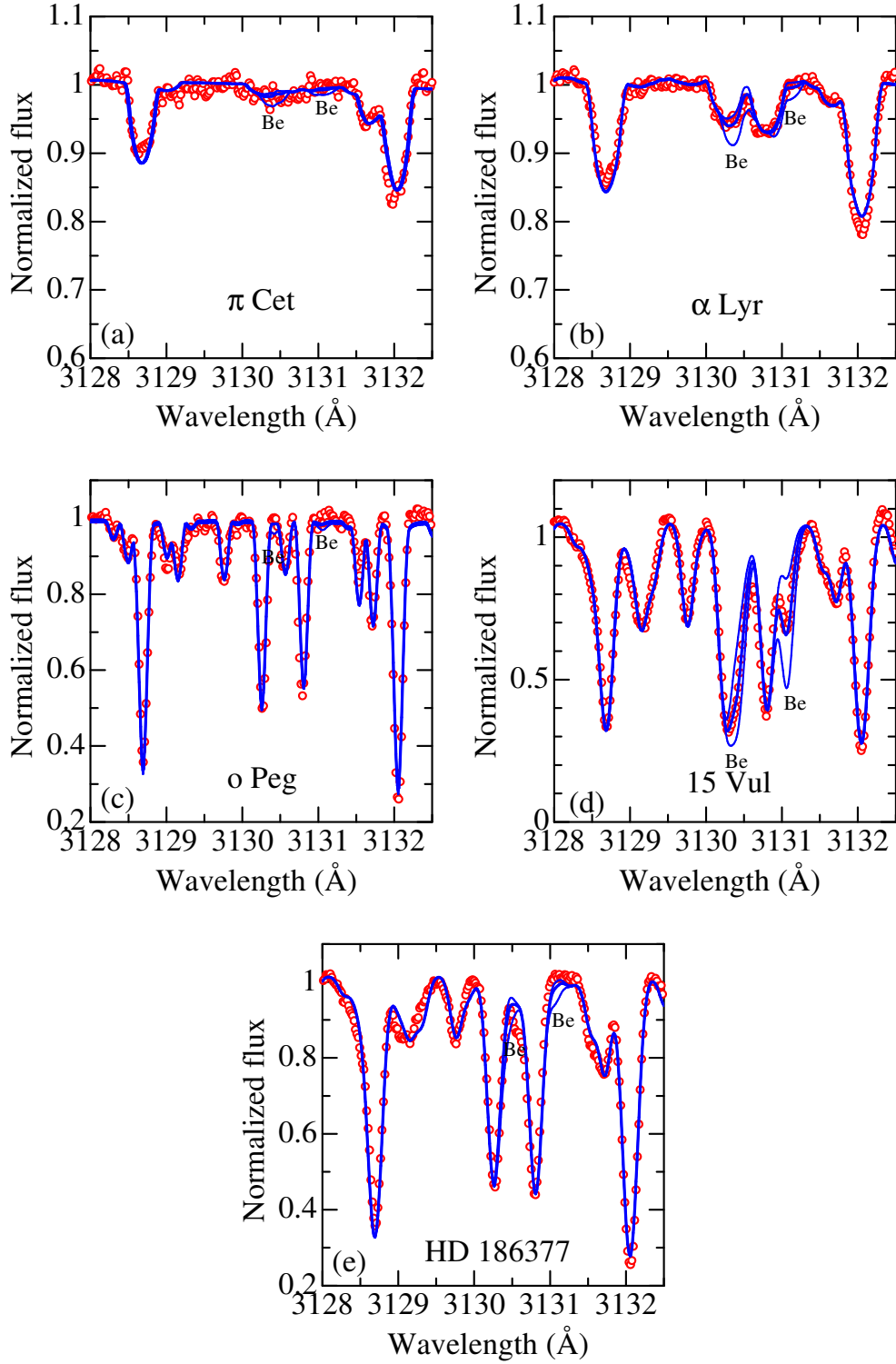


Fig. 10. Synthetic spectrum fitting in the 3128–3132.5 Å region for five late B–late A stars. The thick solid line shows the best-fit theoretical spectrum corresponding to the final Be abundance (given in table 2), while those resulting from perturbing $A(\text{Be})$ by ± 0.5 dex around this solution are shown by thin solid lines. The observed spectrum is depicted plotted by open circles. (a) π Cet, (b) α Lyr, (c) o Peg, (d) 15 Vul, and (e) HD 186377.

Table 1. Basic parameters of the program stars and the results of Be abundances.

HD#	T_{eff} (K)	$\log g$ (cm s^{-2})	v_t (km s^{-1})	[Fe/H] (dex)	$v_e \sin i$ (km s^{-1})	M (M_{\odot})	$\log age$ (yr)	$EW_{\text{BeII } 3131}$ ($\text{m}\text{\AA}$)	$A(\text{Be})$ (dex)	class	S/N	ew^{DL} ($\text{m}\text{\AA}$)	Remark
000087	5072	2.63	1.35	-0.07	3.6	2.74	8.66	33.9	-0.22	a	67	3.1	
000360	4850	2.62	1.34	-0.08	1.9	2.34	8.86	16.6	-0.54	a	63	3.1	
000448	4780	2.51	1.32	0.03	2.0	2.25	8.99	(<4.6)	(<-1.15)	x	43	4.6	
000587	4893	3.08	1.13	-0.09	1.4	1.58	9.36	(<2.2)	(<-1.24)	x	73	2.2	
000645	4880	3.03	1.18	0.07	1.8	1.95	9.08	9.8	-0.52	a	63	2.7	
001239	5114	2.21	1.63	-0.24	4.3	3.75	8.28	56.9	-0.19	a	70	3.2	
002114	5230	2.57	1.57	-0.03	3.3	3.29	8.45	37.5	-0.24	a	87	2.4	
002952	4844	2.67	1.32	0.00	1.9	2.54	8.76	(<3.4)	(<-1.24)	x	56	3.4	PHS
003421	5287	1.88	2.14	-0.20	6.3	4.43	8.13	(<4.0)	(<-1.81)	x	85	4.0	
003546	4882	2.09	1.44	-0.67	3.1	2.00	8.95	11.5	-1.27	a	83	2.4	
003817	5041	2.52	1.40	-0.12	2.5	2.81	8.62	27.4	-0.42	a	74	2.6	
003856	4766	2.28	1.35	-0.15	1.6	3.09	8.55	53.8	+0.02	a	51	3.9	
004188	4844	2.58	1.32	-0.01	2.1	2.54	8.75	(<3.5)	(<-1.27)	x	55	3.5	
004398	4892	2.56	1.37	-0.18	1.9	2.59	8.72	10.2	-0.87	a	60	3.2	
004440	4842	2.91	1.15	-0.10	1.5	1.81	9.19	(<3.8)	(<-1.08)	x	43	3.8	
004627	4599	2.05	1.40	-0.20	1.8	3.06	8.56	(<3.3)	(<-1.57)	x	59	3.3	
004732	4959	3.16	1.12	0.01	1.5	1.74	9.24	(<2.8)	(<-1.08)	x	59	2.8	PHS
005395	4774	2.17	1.40	-0.45	1.2	1.95	9.08	31.4	-0.57	a	55	3.5	
005608	4854	3.03	1.08	0.06	1.4	1.55	9.40	(<2.4)	(<-1.16)	x	74	2.4	PHS
005722	4893	2.49	1.39	-0.23	1.8	2.26	8.95	10.9	-0.90	a	77	2.4	
006186	4829	2.30	1.35	-0.31	1.8	2.30	8.92	12.7	-0.94	a	79	2.5	
007087	4908	2.39	1.53	-0.04	2.9	3.83	8.28	49.9	-0.01	a	77	2.7	
009057	4883	2.49	1.37	0.04	2.3	2.56	8.78	(<2.8)	(<-1.42)	x	68	2.8	
009408	4746	2.21	1.40	-0.34	1.2	2.04	9.00	9.0	-1.15	b	58	3.4	
009774	4980	2.50	1.60	0.02	5.6	3.25	8.46	55.7	+0.13	a	53	4.8	
010348	4931	2.55	1.56	0.01	3.1	3.04	8.54	10.3	-0.82	a	68	3.0	
010761	4952	2.43	1.43	-0.05	2.6	3.04	8.53	11.3	-0.87	a	65	3.1	
010975	4866	2.47	1.37	-0.17	1.7	2.19	8.94	4.2	-1.33	b	71	2.6	
011037	4862	2.45	1.33	-0.14	1.7	2.30	8.88	17.9	-0.63	a	65	2.9	
011949	4845	2.85	1.17	-0.10	1.3	2.17	8.94	24.8	-0.19	a	65	2.7	
012139	4833	2.53	1.36	-0.09	1.7	2.45	8.87	(<2.8)	(<-1.43)	x	68	2.8	
012339	5011	2.52	1.51	-0.03	2.8	3.19	8.48	(<2.5)	(<-1.53)	x	80	2.5	
013468	4893	2.54	1.34	-0.16	1.6	2.31	8.92	24.2	-0.43	a	61	3.2	
013994	4974	2.44	1.83	-0.11	10.1	3.84	8.28	49.6	-0.06	a	49	7.2	
014129	4936	2.61	1.37	-0.01	2.5	2.70	8.68	(<2.8)	(<-1.39)	x	64	2.8	
014770	4977	2.47	1.47	0.01	2.5	3.03	8.54	29.7	-0.33	a	121	1.6	
015779	4846	2.63	1.26	0.00	1.8	2.49	8.78	(<3.2)	(<-1.29)	x	62	3.2	PHS
015920	5061	2.74	1.33	-0.06	3.2	2.63	8.71	33.7	-0.15	a	53	3.8	
016400	4785	2.35	1.33	-0.06	1.8	2.43	8.82	(<3.6)	(<-1.39)	x	55	3.6	PHS
016901	5624	1.42	3.17	0.00	8.7	4.03	8.21	(<6.1)	(<-1.72)	x	74	6.1	
017656	5100	2.67	1.37	-0.06	2.6	2.73	8.66	12.7	-0.74	a	81	2.5	
017824	5051	2.82	1.19	-0.04	3.2	2.37	8.83	41.4	+0.05	a	55	3.5	
018474	5013	2.38	1.42	-0.23	2.6	3.59	8.33	(<3.2)	(<-1.58)	x	61	3.2	
018953	5029	2.93	1.23	0.14	2.5	2.53	8.74	(<3.2)	(<-1.12)	x	60	3.2	
018970	4791	2.44	1.30	-0.07	2.1	2.44	8.81	1.6	-1.70	c	62	3.2	
019476	4933	2.82	1.24	0.14	2.3	2.36	8.83	(<2.9)	(<-1.19)	x	65	2.9	
092125	5468	2.22	2.07	0.03	6.4	3.72	8.30	(<6.6)	(<-1.34)	x	52	6.6	

Table 1. (Continued)

HD#	T_{eff} (K)	$\log g$ (cm s^{-2})	v_t (km s^{-1})	[Fe/H] (dex)	$v_e \sin i$ (km s^{-1})	M (M_{\odot})	$\log \text{age}$ (yr)	$EW_{\text{BeII } 3131}$ ($\text{m}\text{\AA}$)	$A(\text{Be})$ (dex)	class	S/N	ew^{DL} ($\text{m}\text{\AA}$)	Remark
093291	5039	2.74	1.28	-0.10	2.8	2.43	8.79	(<4.7)	(< -1.16)	x	39	4.7	
106057	4956	2.64	1.35	-0.10	1.9	3.06	8.52	(<3.1)	(< -1.37)	x	57	3.1	
106714	4933	2.57	1.37	-0.18	1.8	2.50	8.79	16.5	-0.65	a	60	3.1	
107383	4841	2.51	1.38	-0.28	1.8	3.14	8.49	(<3.0)	(< -1.48)	x	56	3.0	PHS
107950	5171	2.60	1.63	0.01	5.4	3.36	8.42	(<4.6)	(< -1.25)	x	51	4.6	
108225	4969	2.71	1.27	0.04	2.8	2.50	8.77	7.0	-0.91	b	64	3.1	
109272	5104	3.22	1.13	-0.26	1.6	1.79	9.16	6.5	-0.80	b	52	3.0	
109317	4866	2.61	1.38	-0.05	1.7	2.41	8.82	(<3.6)	(< -1.27)	x	52	3.6	
110646	5067	3.05	1.21	-0.45	1.1	1.81	9.12	(<2.2)	(< -1.45)	x	70	2.2	
111028	4881	3.27	1.03	-0.05	0.7	1.41	9.53	(<2.6)	(< -1.03)	x	57	2.6	
113095	4961	2.68	1.37	-0.07	2.1	2.59	8.73	6.6	-1.00	b	55	3.1	
113226	5044	2.63	1.41	0.07	3.0	2.70	8.68	16.6	-0.55	a	45	4.4	
114256	4858	2.68	1.34	0.04	2.0	2.51	8.77	12.3	-0.62	b	42	4.2	
115659	5019	2.47	1.47	-0.06	3.9	2.94	8.57	54.0	+0.04	a	44	4.5	
116957	4898	2.63	1.33	-0.10	1.5	2.39	8.87	8.7	-0.88	b	53	3.3	
117818	4811	2.31	1.34	-0.34	1.9	2.05	9.06	18.2	-0.76	a	51	3.5	
118219	4831	2.34	1.33	-0.34	1.5	2.51	8.74	9.1	-1.10	b	51	3.7	
119126	4796	2.33	1.34	-0.12	1.6	2.38	8.85	2.8	-1.54	b	73	2.6	
119605	5456	1.96	1.95	-0.31	6.6	4.04	8.19	10.2	-1.38	b	57	6.1	
120048	5014	2.79	1.22	0.11	3.5	2.71	8.66	54.5	+0.32	a	58	3.6	
120420	4791	2.63	1.26	-0.20	0.7	2.25	8.90	10.6	-0.78	a	80	2.2	
120787	4843	2.31	1.34	-0.38	1.8	2.02	9.08	22.5	-0.67	a	49	4.1	
125454	4848	2.56	1.39	-0.10	1.8	2.47	8.82	6.2	-1.06	b	56	3.5	
126218	5025	2.50	1.58	0.12	3.5	3.15	8.48	26.0	-0.35	a	43	5.1	
127243	4893	2.21	1.48	-0.77	3.4	1.92	9.08	11.3	-1.25	a	77	2.6	
129312	4993	2.53	1.62	0.01	5.9	4.20	8.15	61.3	+0.22	a	71	3.9	
129336	4901	2.54	1.33	-0.25	2.3	2.68	8.67	(<2.2)	(< -1.62)	x	85	2.2	
129944	4892	2.50	1.32	-0.26	2.0	2.59	8.70	(<2.5)	(< -1.58)	x	69	2.5	
129972	4976	2.69	1.43	-0.01	3.2	2.68	8.69	23.2	-0.35	a	77	2.5	
130952	4750	2.34	1.35	-0.40	4.3	1.85	9.10	10.7	-1.01	a	81	2.7	
131530	4962	2.72	1.33	0.00	2.7	2.72	8.67	15.9	-0.52	a	51	3.9	
132146	5012	2.29	1.60	-0.06	2.8	3.45	8.39	5.1	-1.34	b	72	2.8	
133208	5001	2.35	1.61	-0.07	3.1	3.42	8.40	50.9	-0.08	a	140	1.5	
133392	4903	2.69	1.32	0.09	2.2	2.49	8.77	(<2.3)	(< -1.38)	x	82	2.3	
134190	4841	2.28	1.40	-0.41	1.5	2.03	8.99	(<2.0)	(< -1.85)	x	92	2.0	
136512	4749	2.34	1.39	-0.29	2.3	2.13	8.93	9.2	-1.04	b	59	3.3	PHS
136956	5031	2.61	1.54	0.08	3.0	3.78	8.27	(<4.5)	(< -1.18)	x	48	4.5	
138716	4830	3.14	1.05	0.00	1.3	1.44	9.51	(<2.4)	(< -1.10)	x	66	2.4	
138852	4900	2.55	1.36	-0.22	2.0	2.21	8.98	17.2	-0.64	a	46	3.9	
138905	4822	2.56	1.27	-0.30	1.5	2.15	9.01	46.2	-0.03	a	62	2.9	
139641	4907	2.75	1.16	-0.53	0.7	1.43	9.50	5.2	-1.22	b	68	2.3	
141680	4770	2.32	1.34	-0.24	1.9	2.17	8.95	2.8	-1.58	b	88	2.1	PHS
142091	4877	3.21	1.04	0.10	1.2	1.51	9.43	(<1.6)	(< -1.22)	x	107	1.6	PHS
142198	4760	2.35	1.39	-0.27	1.7	2.13	9.02	(<2.4)	(< -1.64)	x	79	2.4	
142531	4961	2.78	1.37	0.05	2.4	2.64	8.70	(<3.8)	(< -1.14)	x	50	3.8	
143553	4805	2.85	1.17	-0.23	0.7	1.75	9.20	28.7	-0.14	a	54	3.0	
144608	5266	2.54	1.60	-0.09	3.5	3.27	8.45	26.8	-0.49	a	89	2.3	
145001	5119	2.90	1.57	0.04	8.8	3.17	8.49	38.5	+0.04	a	112	2.9	

Table 1. (Continued)

HD#	T_{eff} (K)	$\log g$ (cm s^{-2})	v_t (km s^{-1})	[Fe/H] (dex)	$v_e \sin i$ (km s^{-1})	M (M_{\odot})	$\log \text{age}$ (yr)	$EW_{\text{BeII } 3131}$ ($\text{m}\text{\AA}$)	$A(\text{Be})$ (dex)	class	S/N	ew^{DL} ($\text{m}\text{\AA}$)	Remark
146791	4931	2.69	1.34	-0.07	2.6	2.52	8.78	18.2	-0.48	a	78	2.5	
147677	4978	2.90	1.28	0.10	2.4	2.36	8.83	(<1.6)	(< -1.45)	x	118	1.6	
147700	4843	2.48	1.31	-0.11	1.7	2.35	8.89	29.1	-0.32	a	70	2.7	
148387	5055	2.82	1.34	-0.04	2.6	2.55	8.74	6.2	-0.97	b	59	3.2	
148604	5120	2.90	0.98	-0.16	2.4	2.48	8.76	35.8	-0.07	a	62	3.6	
148786	5110	2.69	1.52	0.17	5.2	2.96	8.55	26.1	-0.25	a	80	2.8	
150030	4850	2.10	1.81	-0.09	4.0	4.02	8.22	4.8	-1.44	b	69	3.3	
150997	5045	2.79	1.26	-0.15	2.7	2.41	8.80	(<1.4)	(< -1.68)	x	135	1.4	
152815	4859	2.43	1.35	-0.21	1.8	2.19	8.93	11.1	-0.91	a	63	3.0	
154084	4862	2.62	1.41	-0.16	2.0	2.39	8.89	(<2.7)	(< -1.43)	x	68	2.7	
154779	5064	2.75	1.44	0.12	3.1	2.79	8.63	4.6	-1.08	b	51	3.8	
156874	4982	2.85	1.32	0.00	2.5	2.53	8.76	(<2.3)	(< -1.35)	x	80	2.3	
156891	4981	2.95	1.30	0.13	3.0	2.44	8.79	(<3.2)	(< -1.10)	x	62	3.2	
157527	5090	2.96	1.30	0.07	3.2	2.49	8.77	(<3.8)	(< -1.07)	x	55	3.8	
158974	4901	2.32	1.43	-0.07	3.0	2.74	8.66	20.3	-0.62	a	86	2.3	
159181	5153	1.50	2.69	-0.15	7.5	4.65	8.09	(<6.7)	(< -1.73)	x	68	6.7	
159353	4919	2.76	1.32	0.00	2.2	2.69	8.69	6.8	-0.89	b	65	2.8	
160781	4593	2.10	1.62	-0.02	4.9	4.99	8.00	115.0	+1.18	a	40	6.5	
161178	4766	2.33	1.32	-0.20	1.8	2.14	8.94	(<4.7)	(< -1.33)	x	40	4.7	
162076	5018	2.98	1.24	0.04	3.1	2.27	8.89	40.7	+0.17	a	63	3.3	
163532	4689	2.17	1.44	-0.06	2.2	3.17	8.55	(<4.4)	(< -1.36)	x	44	4.4	
163917	4928	2.63	1.46	0.13	3.2	3.04	8.52	(<3.4)	(< -1.23)	x	60	3.4	PHS
165760	4962	2.52	1.41	-0.01	2.8	2.82	8.63	11.0	-0.82	a	75	2.6	
167042	4943	3.28	1.07	0.00	0.7	1.50	9.45	(<2.5)	(< -1.05)	x	66	2.5	PHS
167768	4895	2.13	1.44	-0.70	4.4	2.07	8.90	24.0	-0.89	a	76	2.8	
168656	5045	2.66	1.30	-0.06	2.6	2.86	8.60	25.3	-0.36	a	85	2.3	
168723	4972	3.12	1.17	-0.18	1.5	1.84	9.14	(<2.1)	(< -1.30)	x	82	2.1	
170474	4978	2.83	1.29	0.02	2.1	2.47	8.78	(<2.4)	(< -1.33)	x	75	2.4	
171391	5057	2.79	1.23	-0.02	3.2	2.84	8.62	43.1	+0.06	a	69	2.9	
174980	5008	2.71	1.41	0.10	2.8	2.81	8.62	(<4.3)	(< -1.12)	x	45	4.3	
176598	5018	2.83	1.21	0.03	4.3	2.52	8.76	57.1	+0.35	a	56	4.1	
176707	4777	2.27	1.38	-0.29	1.0	2.01	9.03	19.4	-0.72	a	70	2.6	
177241	4906	2.70	1.36	0.01	2.1	2.63	8.71	(<3.4)	(< -1.23)	x	57	3.4	
177249	5251	2.55	1.65	0.00	5.7	3.12	8.51	22.2	-0.55	a	106	2.3	
180540	4951	2.34	1.76	-0.08	5.2	4.34	8.11	25.0	-0.53	a	55	4.6	
180711	4885	2.62	1.38	-0.13	1.6	2.32	8.91	14.2	-0.65	a	67	2.7	
181276	4986	2.78	1.32	0.04	2.0	2.41	8.81	8.8	-0.77	a	81	2.3	
182694	5067	2.63	1.37	-0.04	3.3	2.67	8.69	40.0	-0.10	a	83	2.5	
182762	4872	2.57	1.34	-0.07	1.8	2.42	8.82	9.4	-0.85	a	69	2.7	
183491	4901	2.63	1.40	0.11	2.7	3.07	8.51	1.9	-1.49	c	67	3.2	
184010	5011	3.17	1.16	-0.14	1.3	1.82	9.16	9.2	-0.60	a	81	1.9	
185018	5467	1.85	2.31	-0.10	7.0	4.76	8.06	(<5.2)	(< -1.66)	x	73	5.2	
185194	4978	2.44	1.54	0.03	3.2	3.09	8.52	52.6	+0.05	a	70	3.0	
185351	5006	3.16	1.15	0.00	1.3	1.76	9.23	(<1.9)	(< -1.27)	x	90	1.9	
185467	4937	2.70	1.45	0.13	2.6	2.83	8.61	(<4.8)	(< -1.04)	x	39	4.8	
185758	5535	2.39	1.87	0.01	5.4	4.11	8.18	3.5	-1.55	b	92	3.2	
185958	4876	2.22	2.08	0.02	8.6	4.33	8.11	4.4	-1.38	c	60	5.1	
186675	4953	2.46	1.47	-0.08	2.9	2.74	8.66	(<1.7)	(< -1.74)	x	116	1.7	

Table 1. (Continued)

HD#	T_{eff} (K)	$\log g$ (cm s^{-2})	v_t (km s^{-1})	[Fe/H] (dex)	$v_e \sin i$ (km s^{-1})	M (M_{\odot})	$\log \text{age}$ (yr)	$EW_{\text{BeII } 3131}$ ($\text{m}\text{\AA}$)	$A(\text{Be})$ (dex)	class	S/N	ew^{DL} ($\text{m}\text{\AA}$)	Remark
187739	4771	2.71	1.03	-0.19	2.3	2.01	9.08	67.7	+0.52	a	54	4.2	
188310	4802	2.72	1.42	-0.18	3.8	2.29	8.89	(<3.6)	(< -1.23)	x	56	3.6	PHS
188650	5450	1.79	2.17	-0.67	7.2	4.64	8.07	(<3.4)	(< -2.08)	x	99	3.4	
188947	4866	2.69	1.35	0.07	2.1	2.56	8.74	11.2	-0.65	a	60	3.2	
189127	4760	2.28	1.41	-0.22	1.8	2.31	8.92	19.5	-0.68	a	54	3.7	
192787	5025	2.86	1.25	-0.07	2.1	2.47	8.77	16.7	-0.47	a	90	2.0	
192879	4886	2.62	1.37	-0.09	1.6	2.47	8.83	3.0	-1.36	c	44	4.4	
192944	4981	2.48	1.48	-0.06	3.7	3.41	8.40	37.6	-0.20	a	61	3.7	
192947	5046	2.90	1.32	0.03	3.0	2.43	8.80	31.7	-0.05	a	65	3.1	
194013	4906	2.63	1.32	-0.07	2.3	2.36	8.84	5.9	-1.05	b	69	2.6	
194577	5028	2.68	1.34	-0.02	4.6	3.35	8.43	(<3.1)	(< -1.35)	x	68	3.1	
196857	4878	2.55	1.44	-0.27	1.7	2.15	9.01	23.4	-0.49	a	52	3.7	
199665	4985	2.84	1.19	-0.05	2.7	2.25	8.90	(<2.7)	(< -1.31)	x	70	2.7	PHS
200039	4965	2.67	1.36	-0.13	2.0	2.62	8.70	4.2	-1.24	b	49	3.7	
201381	4951	2.77	1.30	-0.04	2.4	2.35	8.85	13.0	-0.60	a	61	3.1	
203222	5067	2.78	1.29	-0.02	2.2	2.49	8.77	5.7	-1.02	b	73	2.5	
203387	5244	3.07	1.26	0.07	5.3	2.79	8.63	26.5	-0.12	a	63	3.8	
204381	5100	2.84	1.33	-0.06	2.4	2.47	8.78	14.0	-0.59	a	60	3.2	
204771	4967	2.93	1.26	0.09	2.2	2.44	8.79	(<3.4)	(< -1.09)	x	53	3.4	
205072	4995	2.72	1.34	-0.14	2.1	2.41	8.80	(<4.5)	(< -1.19)	x	30	4.5	
205435	5114	3.00	1.20	-0.10	3.1	2.33	8.85	31.8	-0.07	a	59	3.4	
206356	4938	2.80	1.28	0.11	2.3	2.55	8.74	15.7	-0.42	a	52	3.8	
206453	5038	2.43	1.48	-0.38	2.4	2.97	8.53	13.4	-0.95	a	66	2.9	
209396	4999	2.81	1.30	0.04	3.1	2.46	8.79	12.7	-0.58	a	71	2.8	
210354	4793	2.36	1.39	-0.22	3.0	1.92	9.12	(<3.1)	(< -1.52)	x	62	3.1	
210434	4949	2.93	1.36	0.12	2.7	2.29	8.87	16.3	-0.33	a	70	2.6	
210702	4967	3.19	1.10	0.01	2.0	1.68	9.28	(<2.2)	(< -1.17)	x	76	2.2	PHS
210807	5071	2.58	1.57	-0.10	6.7	3.50	8.37	31.6	-0.31	a	51	5.2	
211391	4909	2.57	1.36	0.09	2.3	2.78	8.64	11.8	-0.69	a	59	3.4	
211434	5082	2.70	1.37	-0.26	1.9	2.53	8.73	13.5	-0.76	a	77	2.3	
211554	5043	2.41	1.63	0.05	3.8	4.26	8.12	26.8	-0.43	a	70	3.1	
212271	5002	2.90	1.21	0.10	2.6	2.50	8.76	44.4	+0.22	a	50	3.9	
212320	5075	2.59	1.46	-0.11	3.5	2.84	8.61	54.6	+0.08	a	76	2.8	
212430	4954	2.56	1.39	-0.17	2.0	3.17	8.49	16.7	-0.65	a	58	3.2	
212496	4710	2.43	1.22	-0.33	1.4	1.85	9.12	(<3.2)	(< -1.47)	x	57	3.2	
213789	5010	2.73	1.37	-0.06	2.6	2.77	8.64	8.8	-0.85	a	67	2.9	
213930	5011	2.87	1.34	0.12	4.2	2.75	8.65	58.9	+0.45	a	54	4.3	
213986	4928	2.83	1.27	0.08	2.1	2.50	8.76	7.6	-0.77	b	54	3.7	
214567	4989	2.69	1.33	-0.21	2.6	2.57	8.71	10.4	-0.85	a	83	2.3	
214878	5041	2.85	1.29	0.04	2.4	2.62	8.71	1.7	-1.48	c	58	3.3	
215030	4731	2.41	1.25	-0.49	0.7	1.83	9.24	4.8	-1.37	b	63	2.8	
215373	5007	2.69	1.39	0.10	3.7	2.66	8.69	12.0	-0.65	a	66	3.1	
215721	4829	2.23	1.39	-0.48	1.0	1.95	9.07	8.7	-1.23	b	65	2.9	
215943	4878	2.68	1.33	-0.04	1.9	2.45	8.84	(<3.2)	(< -1.28)	x	60	3.2	
216131	5000	2.69	1.24	-0.05	2.2	2.49	8.77	9.7	-0.82	a	64	2.9	
217264	4946	2.80	1.27	0.12	2.0	2.55	8.74	(<2.5)	(< -1.28)	x	75	2.5	
217703	4890	2.91	1.16	-0.17	0.9	1.98	9.05	20.0	-0.32	a	57	3.0	
218527	4935	2.57	1.33	-0.34	3.7	2.11	9.03	(<2.9)	(< -1.53)	x	89	2.9	

Table 1. (Continued)

HD#	T_{eff} (K)	$\log g$ (cm s^{-2})	v_t (km s^{-1})	[Fe/H] (dex)	$v_e \sin i$ (km s^{-1})	M (M_{\odot})	$\log age$ (yr)	$EW_{\text{BeII } 3131}$ ($\text{m}\text{\AA}$)	$A(\text{Be})$ (dex)	class	S/N	ew^{DL} ($\text{m}\text{\AA}$)	Remark
219139	4860	2.50	1.38	-0.19	2.0	2.29	8.88	4.6	-1.27	b	64	2.9	
219615	4802	2.25	1.37	-0.62	1.7	1.67	9.20	24.8	-0.73	a	63	3.0	
219945	4874	2.61	1.36	-0.10	1.7	2.57	8.77	5.2	-1.12	b	70	2.7	
221345	4813	2.63	1.43	-0.24	2.6	2.20	8.93	(<3.1)	(<-1.38)	x	65	3.1	PHS
222093	4853	2.56	1.38	-0.12	2.0	2.28	8.89	(<3.8)	(<-1.29)	x	51	3.8	
222387	5055	2.81	1.22	-0.11	2.7	2.79	8.63	38.8	-0.03	a	44	5.1	
222574	5523	1.99	2.20	0.04	7.0	4.23	8.13	(<5.4)	(<-1.54)	x	69	5.4	
223252	5031	2.72	1.34	-0.03	2.8	2.52	8.76	13.0	-0.66	a	65	2.9	
224533	5030	2.73	1.28	-0.01	2.6	2.54	8.75	13.2	-0.64	a	73	2.6	

Note.

Following the HD number (column 1), the fundamental stellar parameters of the program stars, all of which were taken from Paper I, are given in columns 2–8: the effective temperature, logarithmic surface gravity, microturbulent velocity dispersion, metallicity (logarithmic Fe abundance relative to the Sun), projected rotational velocity, initial stellar mass, and logarithmic stellar age. Columns 9–11 present the results of our abundance analysis: the inversely determined equivalent width of the Be II 3131.07 line, the logarithmic Be abundances (expressed in the usual normalization of $A(\text{H})=12.00$), and the reliability class (cf. subsection 3.2), respectively, where the parenthesized values denote the upper limits (undetermined cases). The spectrum quality-related quantities (S/N ratio at $\lambda \sim 3131 \text{ \AA}$ and the detection-limit equivalent-width defined in subsection 3.2) are given in columns 12 and 13. Planet-harboring stars are denoted as “PHS” in column 14.

Table 2. Error simulation based on artificial spectra.

A_{given}	$\langle A \rangle$ (S/N = 100)	σ	N	$\langle A \rangle$ (S/N = 50)	σ	N	$\langle A \rangle$ (S/N = 20)	σ	N
+1.0	+0.999	0.010	100	+0.999	0.020	100	+0.996	0.050	100
+0.5	+0.502	0.012	100	+0.504	0.024	100	+0.510	0.060	100
0.0	0.000	0.014	100	+0.001	0.028	100	0.000	0.071	100
-0.5	-0.506	0.035	100	-0.515	0.072	100	-0.551	0.195	99
-1.0	-1.012	0.079	100	-1.024	0.145	98	-1.004	0.271	86
-1.5	-1.500	0.236	92	-1.402	0.451	72	-1.107	0.358	61

Note.

Experiment of Be abundance derivations based on many artificial spectra computed with different input Be abundances (+1.0, +0.5, 0.0, -0.5, -1.0, and -1.5) and different S/N ratios (100, 50, and 20). Shown here are the average of resulting abundances ($\langle A \rangle$), the standard deviation (σ ; in dex), and the number of successful determinations (N ; among 100 trials) for each case. See appendix 1 for more details.

Table 3. Be abundance results of five late B–late A stars.

Star	HD#	Sp.Type	T_{eff}	$\log g$	v_t	$A(\text{Be})$	Remark
π Cet	17081	B7 V	13063	3.72	1.0	+0.78:	near to upper limit
α Lyr	172167	A0 V	9435	3.99	2.0	+0.85:	near to upper limit
o Peg	214994	A1 IV	9453	3.64	2.0	+0.05:	near to upper limit
15 Vul	189849	A4 III	7870	3.62	4.0	+1.47	clearly detected
HD 186377	186377	A5 III	7733	2.40	4.0	-0.38 :	near to upper limit, late-A giant

Note.

See appendix 2 for details. The “:” (colon) attached to $A(\text{Be})$ denotes “uncertain value.”